Article in Press: JJEES 16(2), June 2025.
This article has been accepted for publication and will appear in the upcoming issue. The final published version will be available through the journal website after copyediting, typesetting and proofreading. ©2025 JJEES.

Age, Geochemistry, and Petrogenetic Constraints on Ediacaran Granitoids, Southwest Jordan.

Reema Moshtaha[1], Rolf Romer[2], and Ghaleb H. Jarrar[3*]

1. Ministry of Education, Amman, Jordan
2. GeoForschungszentrum-Potsdam, Germany
3. Geology Department, The University of Jordan, P.O.Box 13633, 11942-Amman, Jordan

Received on March 6, 2024, Accepted on January 2, 2025

Abstract

The final stages of the terminal collision between East and West Gondwana at 600 ± 50 Ma ago are characterized by post-collisional calc-alkaline and A-type alkaline granitoids intruding the Neoproterozoic basement in southern Jordan. Available U-Pb zircon, Rb-Sr and Sm-Nd mineral and whole-rock age data on these granitoids are inconsistent. To improve constrain the geological relevance and timing of the change in the chemical character of magmatism in the Jordanian basement, the geochemical, mineralogical, isotopic characteristics and dating of representative calc-alkaline (Sabil granodiorite) and A-type alkaline (Feinan, Humrat and Mubarak) granitoids were reevaluated by several geochemical, mineralogical and dating methods. Sabil is a high-K calc-alkaline intermediate intrusion. It shows enrichments of LILE relative to HFSE as well as Sr, Ba, P, Zr, Ti, Cr, Co, and Ni. Further, a well-developed depletion in K, Rb, Th, Ta, Nb, and Y; and a weak E-anomaly (Eu/Eu* = 0.7 - 1.0). The alkaline granitoids display higher SiO2, Na2O+K2O, Fe/Mg, enrichment in Zr, Nb, Y, Rb, Ta, K, and REE contents, with corresponding depletion in CaO, Ba, Sr, Ti, and P along with a pronounced Eu anomaly (Eu/Eu* = 0.06 – 0.85). They show close similarity to within-plate A-type granites. Both of them have LREE-enriched and flat HREE patterns. Nevertheless, the alkaline granites are characterized by higher LREE enrichment and lower MREE and HREE contents, except for the Mubarak unit, which displays a concave upward REE pattern. They also follow a gently sloping LREE and almost flat HREE chondrite-normalized patterns in general, while the calc-alkaline Sabil unit shows a smooth flat to steep chondrite-normalized REE pattern. The U-Pb zircon ages for the Sabil granodiorite unit are about 616 Ma, and 603, 601, and 586 Ma for the Feinan, Mubarak, and Humrat units, respectively. The εNd values of the alkali rocks ranged from + 2.9 to + 5.4 with (0.70146 to 0.715080) initial $^{87}Sr/^{86}Sr$. They overlap with the εNd values of the calc-alkaline rocks (+ 3.7 to + 4.6) with low initial $^{87}Sr/^{86}Sr$ (~ 0.70374). Mineralogical and geochemical characteristics suggest that both rocks were not products of the same magma source. The investigated granitoid could have been produced through decompressional partial melting of the subcontinental lithosphere and lower continent, following slab failure and mantle delamination, with fractional crystallization and minor crustal assimilation. The transitional magmatism (Feinan and Mubarak units) coincides or slightly post-dates with the Araba Unconformity and the extensive dike swarms.

Keywords: Arabian-Nubian Shield, Jordan, U-Pb zircon geochronology, granitoids, geochemistry.

* Corresponding author's email address: jarrargh@ju.edu.jo

Article in Press: JJEES 16(2), June 2025.
This article has been accepted for publication and will appear in the upcoming issue. The final published version will be available through the journal website after copyediting, typesetting and proofreading.

1. Introduction

The continental crust, which is mainly made of granitoids, cannot be directly derived from the mantle through partial melting due to disequilibrium between the felsic melts and the ultramafic mineral assemblage of the mantle (e.g., Johannes and Holtz, 1996). Hence, two principal mechanisms and derivatives, thereof, are invoked for the generation of the granitoid magmas: differentiation by fractional crystallization with or without crustal contamination of mantle-derived mafic magmas and water, or hydrous minerals, assisted by partial melting of felsic, meta-igneous and metasedimentary rocks (Moyen et al., 2017). The first mechanism contributes to crustal growth, while the second just recycles pre-existing crustal rocks (e.g., Tang et al., 2020).

The Arabian-Nubian Shield (ANS) is the northern segment of East African Orogen (EAO, ~ 900 to 530 Ma, Stern, 1994) that extends from south to north for about 6000 km and represents one of the largest juvenile continental crust exposures on Earth. The EAO combines two types of mobile orogenic belts: juvenile volcanic arc terranes of the ANS and the lower crustal associated remnants of the Mozambique belt. The former, according to Kröner and Stern (2004), comprises Neoproterozoic supracrustal and magmatic assemblages including ophiolites, subduction or collision-related granitoids, while the latter is made of poly-metamorphosed high-grade metamorphic assemblages, with protoliths predominantly of Mesoproterozoic to Archean continental crust as well as the reworked Neoproterozoic crust (e.g. Boyd et al., 2010).

The juvenile island and volcanic arc terranes of the ANS witnessed, during the EAO, a series of repeated deformational and metamorphic events ranging from greenschist to upper amphibolite facies (e.g. Abu El-Enen and Whitehouse 2013; Habboush and Jarrar 2009; Jarrar et al., 2013a). The above authors and Elisha et al., 2017; 2019 constrained the age of the peak of metamorphism at ~ 620 ± 5 Ma. These processes were associated with and followed by voluminous intrusive and volcanic activities that culminated in the cratonization of the ANS (e.g., Jarrar et al., 2003; Eyal et al., 2010; Johnson et al., 2013).

During the final stages of the amalgamation of the ANS terranes (630-540 Ma), the chemical affinity of the magmatism changed from calc-alkaline to alkaline with a contemporaneous change in tectonic style from collision through post-collision to within plate extension and finally to stable platform setting (Garfunkel, 1999; Kröner and Stern, 2004). El-Bialy and Hassen (2012) documented the onset of anorogenic alkaline magmatism in Sinai at St. Katherina at 590-580 Ma. The wealth of geochronologic data in the last two decades documents intensive and continuous magmatic activity including the gradual transition from calc-alkaline to alkaline magmatism (Eyal et al. 2019). Beyth et al. (1994) suggested that the transition has occurred at ca. 610 Ma. Ibrahim and McCourt (1995), based on field observations and limited geochronological and geochemical data, divided the basement complex of South Jordan into two complexes: the Aqaba and Araba complexes, which are separated by intra Neoproterozoic unconformity that is marked by the deposition of the Saramuj conglomerate. Powell et al. (2015) coined the name Araba Unconformity for this unconformity and placed it at about 605 Ma. It should, however, be noted that the age data for both complexes are scarce and mainly comprise Rb-Sr whole rock data (Brook et al., 1990), Ibrahim and McCourt, 1995; Jarrar et al., 2008). Brook et al. (1990), reported whole-rock Rb-Sr isochrons of 589 ± 36, 538 ± 30, 567± 5, and 560 ± 10 Ma for the Sabil, Feinan, Humrat, and Mubarark units, respectively. Jarrar et al. (2008) reported a whole-rock Rb-Sr age of 558 ± 13 Ma for the Feinan granite. These ages generally overlap and quite often contradict the field observation. Furthermore, there is a scarce U-Pb zircon age for the granitoid of the Neoproterozoic of Jordan, in particular the Araba Complex.

Article in Press: JJEES 16(2), June 2025.
This article has been accepted for publication and will appear in the upcoming issue. The final published version will be available through the journal website after copyediting, typesetting and proofreading. ©2025 JJEES.

Accordingly, this study presents U-Pb conventional age determinations on zircons and titanite as well as detailed geochemical, petrologic, and Sr-Nd-Pd isotope investigations for three granitic units, Feinan, Humrat, and Mubarak, and on the Sabil granodioritic unit from the calc-alkaline batholiths of the Aqaba Complex (Ibrahim and McCourt, 1995).

2. Geologic Setting

The northernmost outcrops of the ANS in South Jordan (Figures. 1 A and B) cover about 1400 sq. km and are dominated by granitoids that intrude into the two principal metamorphic complexes, the Abu-Barqa metasedimentary suite and the Janub Metamorphic Complex in addition to megaxenoliths of amphibolites and biotite-hornblende schists i.e. Abu-Saqa schist (Ibrahim and McCourt, 1995, Jarrar, 1995). The U-Pb ages of the protoliths of the Abu-Barqa metasedimentary suite have been constrained at 680-900 Ma, while the age of the peak of metamorphism was constrained at about 620±5 Ma (Jarrar et al., 2013a; Elisha et al., 2019). Field relationships with cross-cutting granitoids in addition to SIMS U-Pb ages on zircon constrained the age of Janub Metamorphic Complex and the associated magmatic activity between 645-615 ± 5 Ma. The lower limit of 615 Ma coincides with the age of Abu-Barqa Metamorphic Suite (Ghanem et al., 2022).

The Aqaba Complex includes metamorphic and calc-alkaline igneous rocks below the regional peneplain (Ibrahim, 1991,1993). The complex comprises metamorphic rocks, preserved as narrow belts and megaxenoliths, ranging in age from 800-620 Ma, hornblendite and hornblende gabbro, and amphibolites (Jarrar, 1995, 1998), a foliated granitic suite (Rahma Foliated Suite), and four 625-600 Ma old post-orogenic granitoid suites (Darba Tonalitic, Rumman Granodiorite, Urf Porphyritic, and Yutum Granitic Suites). The whole complex is extensively cut by dike swarms of variable compositions and nature i.e. simple, composite, and hybrid (Ghanem et al., 2020; Jarrar et al., 2004, Jarrar et al., 2013b; Wachendorf et al., 1985).
The Araba Complex is bounded by two major unconformities, the Ediacaran Araba Unconformity (~ 605 Ma, as set by Powell et al., 2015) at its base, which truncates the Aqaba Complex lithologies, and the regional lower Cambrian Ram Unconformity (set at ~ 530 Ma; Powell et al, 2014). The latter is marked by the extensive deposition of the lowest member of the Ram siliciclastic sedimentary Group (Ibrahim and McCourt, 1995; Jarrar et al., 2003). The Araba Complex comprises the Safi Group (Saramuj Conglomerate Formation and the Hiayala Volcani-clastic Formation), the magmatic rocks of the Humrat-Feinan Suite, the Araba Mafic to Intermediate Suite, and the Aheimir alkaline to peralkaline rhyolitic Suite. The first two magmatic suites were lumped together as the Araba Alkaline Bimodal Plutonic Suite (Jarrar, et al., 2003). Furthermore, the Araba Complex commences by the deposition of the Safi Group, which comprises the Saramuj Conglomerate, the Haiyala Volcaniclastic, and the Um Gaddah Formations (Powell et al., 2015). Generally speaking, rocks of this complex are exposed along the eastern margin of Wadi Araba in addition to sporadic exposures throughout the basement, east and northeast of Aqaba (Figs. 2 and 3)

This study focuses on the Humrat-Feinan Suite (Mubarak, Feinan, and Humrat alkali-feldspar granites and syenogranites units) and the calc-alkaline Sabil granodiorite unit as a part of the Rumman Granodiorite Suite from the Aqaba complex. The Humrat-Feinan Suite is exposed mainly in a horst block in the Dana area (Feinan, Figure. 2), an area of very rugged terrane, and in places to the east and northeast of Aqaba, e.g., Jabal Humrat, Wadi Yutum, Jabal Mubarak, and Wadi Sabil (Sabit) (Figure. 3). This suite, in particular the Humrat unit, is rarely cut by dikes and presumably represents the felsic end member of the Araba Alkaline Plutonic Bimodal Suite (Jarrar, et al., 2003).

Article in Press: JJEES 16(2), June 2025.
This article has been accepted for publication and will appear in the upcoming issue. The final published version will be available through the journal website after copyediting, typesetting and proofreading.

The Humrat alkali-feldspar granites are the youngest among the investigated granitoids (Jarrar, et al., 2003). Jarrar, et al. (2008) suggested that the Feinan granite could have been derived from the Ghuweir mantle-derived mafics via fractional crystallization depending on their Rb-Sr ages for Araba granites (Humrat 568 Ma; and Feinan 559 Ma), while the mafic rocks cluster at 595 Ma using U-Pb zircon Concordia of the complex suites (Ghanem and Jarrar, 2013; Jarrar and Ghanem, 2021)
The Rumman Granodiorite Suite occurs dominantly in the southeastern part of the granitoid outcrops extending to the south and west from Wadi Rumman to Wadi Sabil down to the Jordan-Saudi Arabia border (Figure. 3). According to McCourt and Ibrahim (1990), the suite comprises four units ranging in composition from diorite to monzogranite.

In the field, these grayish-green units generally have a low relief and are extensively cut by NE-SW trending dike swarms. The age of the suite was determined to be 583 ± 3 Ma with an initial $^{87}Sr/^{86}Sr$ ratio of 0.7035 ± 0.0001 using Rb-Sr whole dating (Brook et al., 1990). Regional petrological correlation with the Midyan area indicates that this Rb-Sr age is too young in comparison to the younger granites exposed in the Eastern Desert of Egypt (McCourt and Ibrahim, 1990)

Article in Press: JJEES 16(2), June 2025.
This article has been accepted for publication and will appear in the upcoming issue. The final published version will be available through the journal website after copyediting, typesetting and proofreading. ©2025 JJEES.

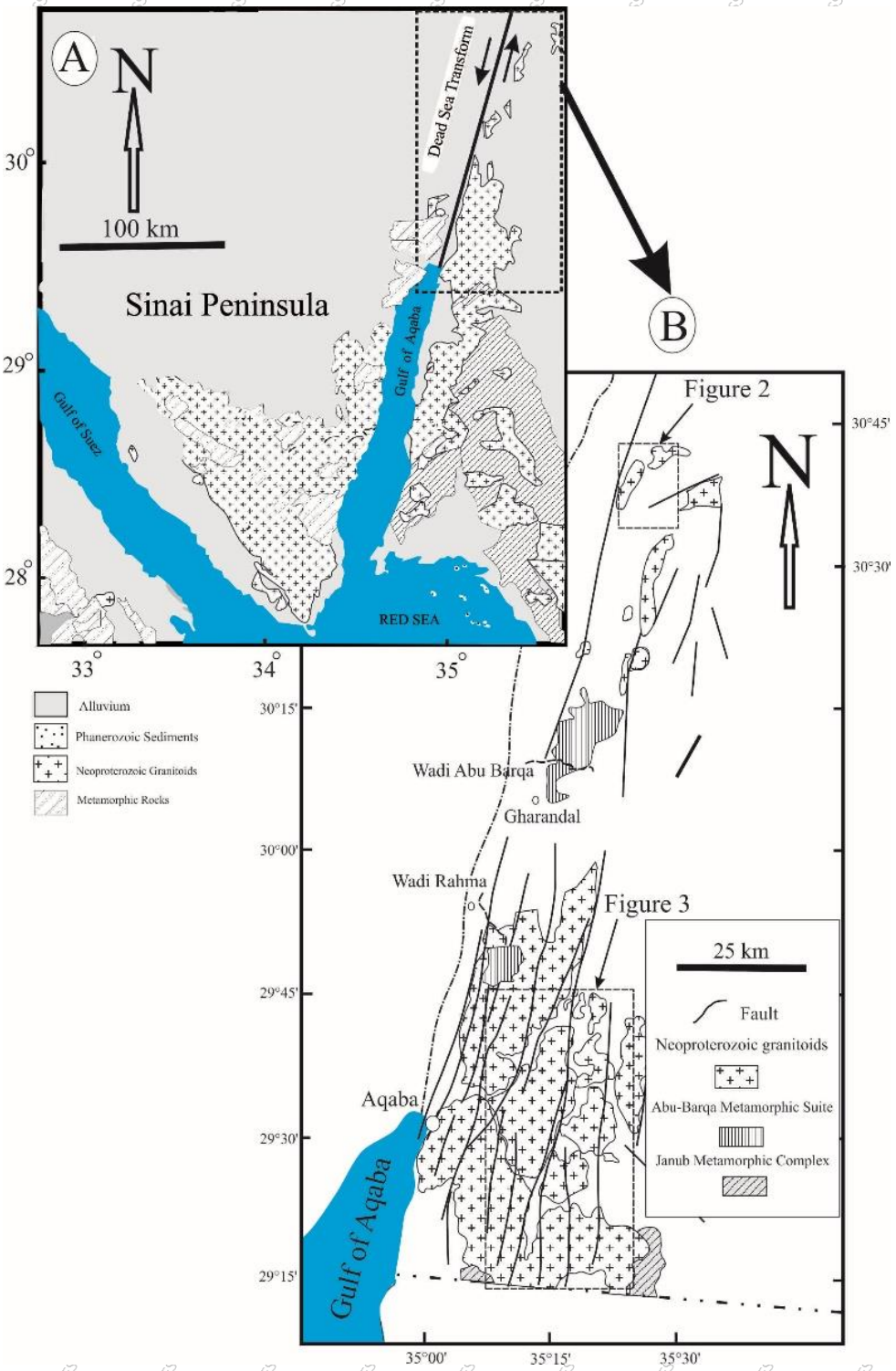

Figure. 1. A. The northernmost exposures of the Arabian-Nubian Shield in Sinai, Jordan, and surrounding areas; **B**. The outcrops of the Neoproterozoic basement in southern Jordan and along the eastern shoulder of Wadi Araba, insets for Figures. 2 and 3 are shown on the map. Slightly modified after Ibrahim and McCourt (1995)

Article in Press: JJEES 16(2), June 2025.
This article has been accepted for publication and will appear in the upcoming issue. The final published version will be available through the journal website after copyediting, typesetting and proofreading. ©2025 JJEES.

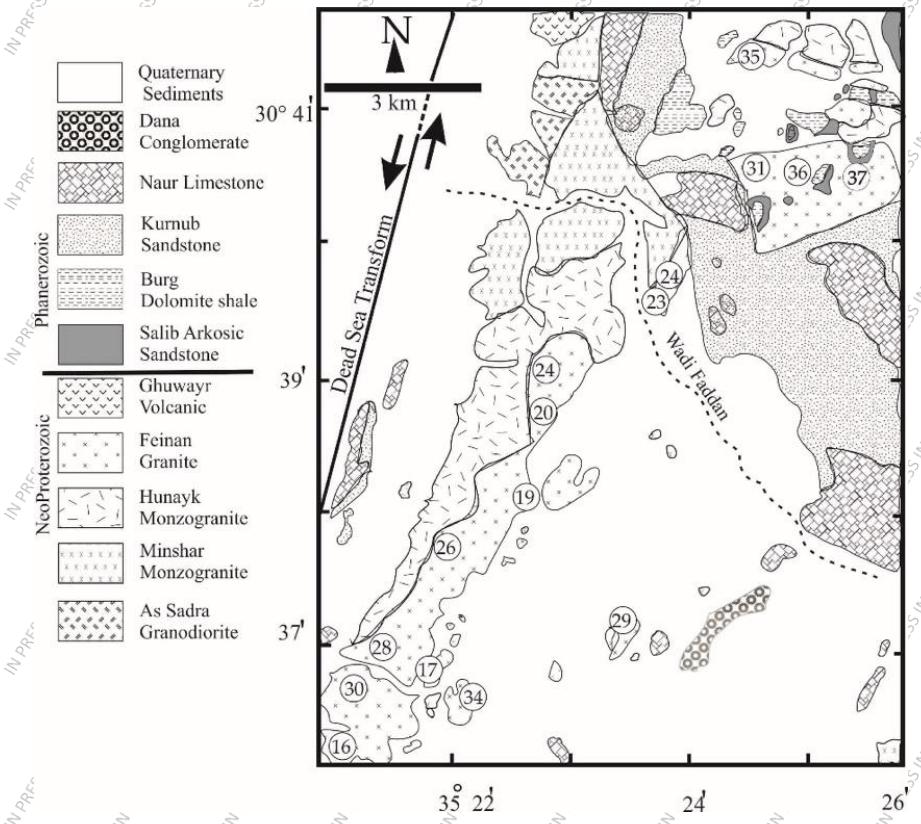

Figure. 2. The outcrops and sample locations of Feinan unit granites in Central Wadi Araba. Other Neoproterozoic basement and Phanerozoic rocks are shown. Modified from Figure 5.2 (Jarrar and Ghanem, 2021)

3. Field and petrographic aspects

In Wadi Marsad in the Quweira area, the Humrat granite carries the Marsad granite of the older Urf suite as roof pendants (Figure. 4A). Further to the south in Wadi Sabil, the Humrat granite intrudes the Sabil granodiorite with a vertical contact, that is typical of shallow intrusions (Figure. 4B). In this area and elsewhere, this granite is rich in miarolitic vugs filled with euhedral quartz and other secondary minerals. The Feinan granites show great similarity to the Humrat granite in hand-specimen, but quite often are white reddish in contrast to the Humrat which is always brick red in color. The reddish colored, simply twinned microperthite dominates over albite plagioclase.

The Humrat unit is alkali feldspar granites to syenogranites that are reddish in color, aphyric, medium to coarse-grained and comprises principally microperthite, albite plagioclase and quartz with occasional biotite and accessories of apatite, zircon, titatnite and fluorite. Micrographic texture is occasionally present between microperthite and quartz (Figure. 5 A&B).

Article in Press: JJEES 16(2), June 2025.
This article has been accepted for publication and will appear in the upcoming issue. The final published version will be available through the journal website after copyediting, typesetting and proofreading.

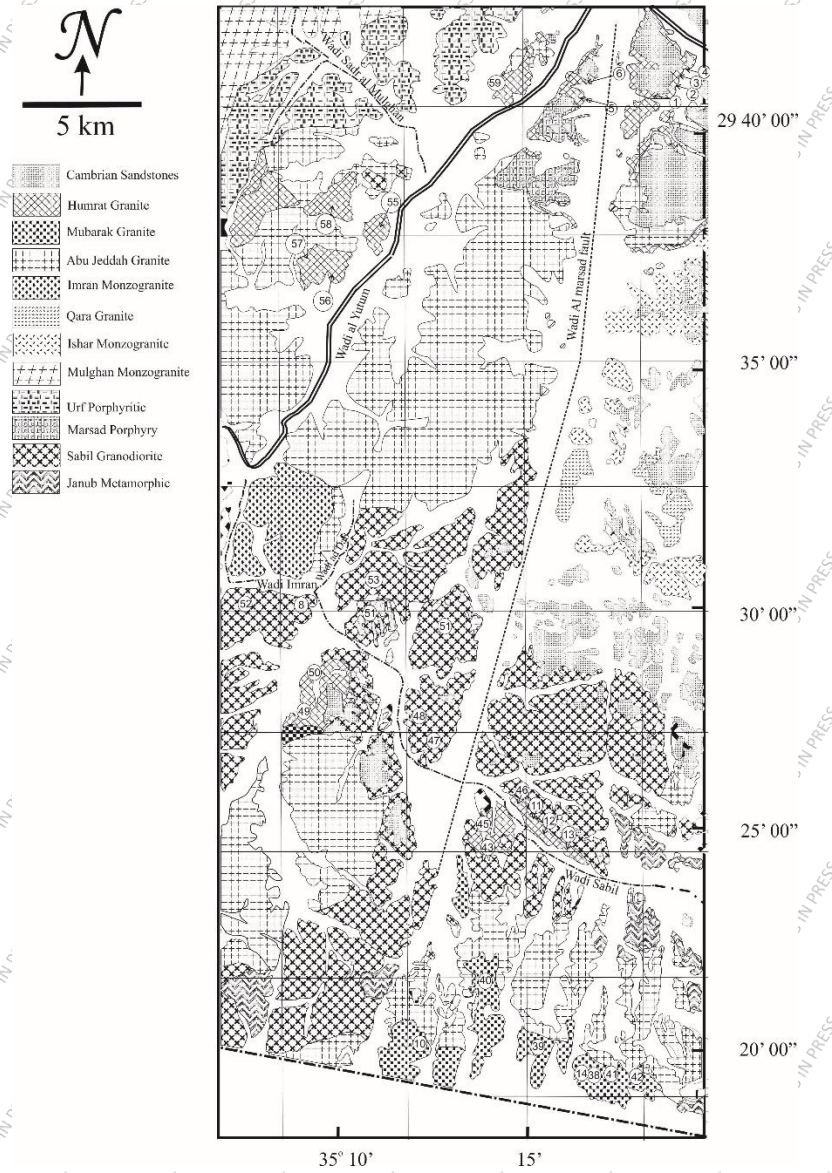

Figure. 3. Distribution and sample locations of Sabil granodiorite, Humrat and Mubarak granites east and northeast of Aqaba. Other units of the Aqaba complex are shown as well. Modified from Figure 5.2 (Jarrar and Ghanem, 2021).

Article in Press: JJEES 16(2), June 2025.
This article has been accepted for publication and will appear in the upcoming issue. The final published version will be available through the journal website after copyediting, typesetting and proofreading. ©2025 JJEES.

Figure. 4. A. The Humrat granite is carrying Marsad granite as roof pendants, and both are truncated by the Ram Unconformity. Note the abundance of dykes in the Marsad granite compared to the dolerite cutting both types of granites**. B**. Humrat granites intruding the Sabil granodiorite with vertical contacts. Note the rhyolite dykes crossing the Sabil granodiorite in the background.

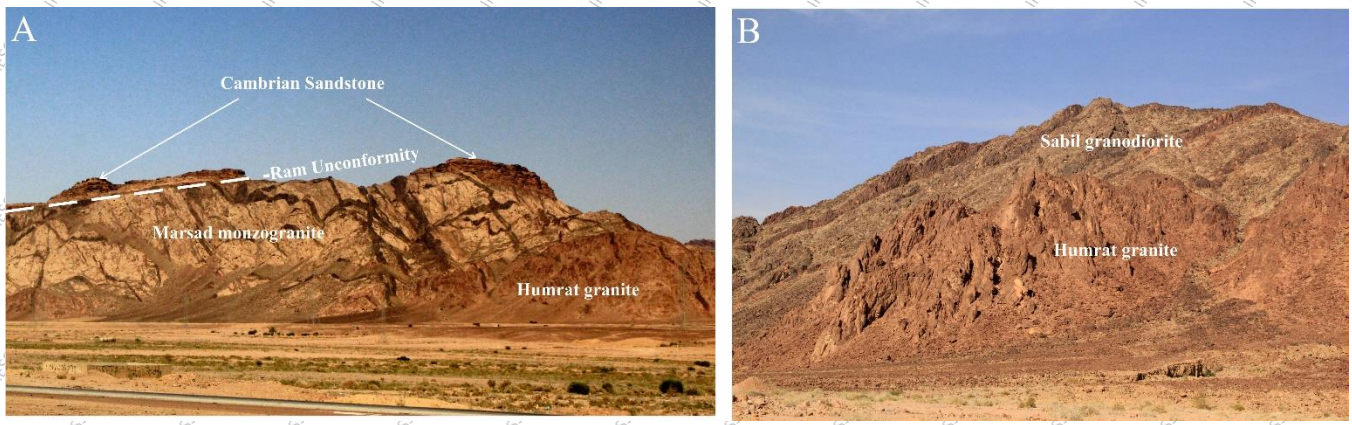

Feinan granite is massive medium to coarse grained and locally pegmatitic. It consists of micro to mesoperthite, albite plagioclase, and quartz as major constituents. Accessories of chloritized biotite, fluorite, zircon, apatite, titanite and opaques. Feinan granite consists of brownish to cloudy microperthite and quartz, with scarce albite (Figure. 5C).

Mubarak granite consists of albite (An ~5%), perthite, and quartz. Scarce biotite and opaque. The Mubarak Monzogranite is coarse-grained to sub-pegmatitic granite with rare aggregates of biotite. The perthite displays the Manebach twin with a typical herringbone pattern of exsolved albite (Figure. 5D).

The Sabil granodiorite is greenish grey weathered medium to coarse-grained granular hypidiomorphic rock with a high color index due to the abundance of hornblende, biotite, and titanite. In the field, it forms low-lying hills relative to the intruding, brick-red alkali feldspar granite of the Humrat unit. Oligoclase is the principal mineral that occurs as subhedral tabular to prismatic grains, complexly twinned, and often with weathered cores. A flow texture is obvious from the arrangement of the

Article in Press: JJEES 16(2), June 2025.
This article has been accepted for publication and will appear in the upcoming issue. The final published version will be available through the journal website after copyediting, typesetting and proofreading.

plagioclase (Figure. 6 A) Quartz is dull grey and occurs with K-feldspar and interstitial milky white plagioclase.

Hornblende is euhedral, brownish green, and strongly pleochroic (Figure. 6B).

Article in Press: JJEES 16(2), June 2025.
This article has been accepted for publication and will appear in the upcoming issue. The final published version will be available through the journal website after copyediting, typesetting and proofreading. ©2025 JJEES.

Figure. 5. A sericitized albite (Ab) and perthite (Per) in Humrat granite (X-Nicols); B. micrographic texture of quartz intergrowth with perthite in Humrat granite (PPL, Sample NF-43); C. Slightly weathered perthite with simple twin in Feinan Granite (X-Nicols, Sample NF-31) ; Herringbone structure in perthite in Mubarak granite (X-Nicols, Sample NF-39).

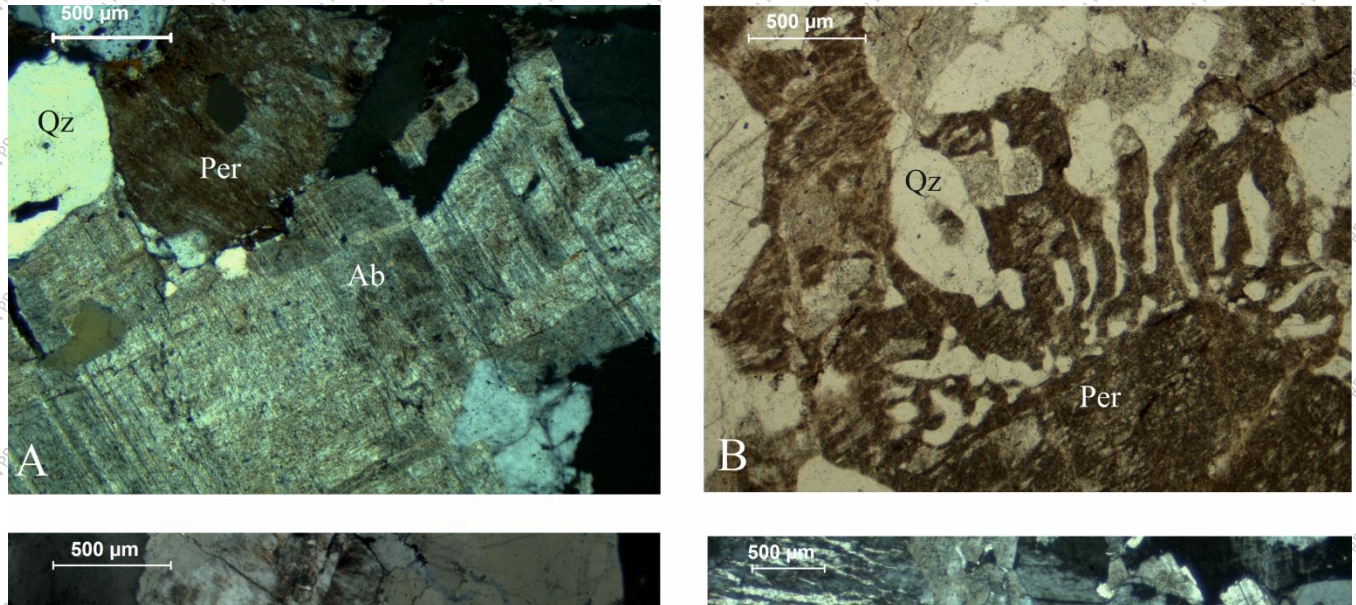

Article in Press: JJEES 16(2), June 2025.
This article has been accepted for publication and will appear in the upcoming issue. The final published version will be available through the journal website after copyediting, typesetting and proofreading. ©2025 JJEES.

Figure. 6. A. whole thin section microphotograph of Sabil granodiorite (X-Nicols, Sample NF-8). Flow texture is well demonstrated by the twinned prismatic oligoclase (PL). Hornblende (Hbl., bioitite (Bt.), and titanite (Tn) form clusters. Some hornblende is rimming augite (Aug). Orthoclase (Or) and quartz (Qz) are interstitial phases. **B.** Enlarged part of A, indicated by the arrow, showing hornblende, titanite quartz, and biotite.

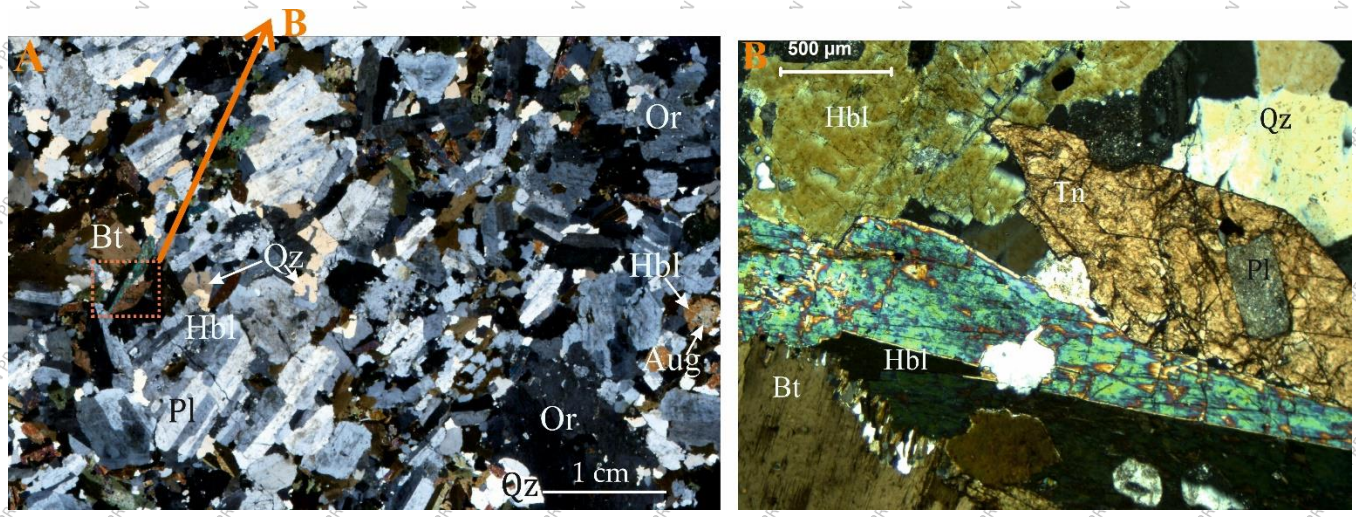

4. Analytical Techniques

Fifty-nine samples were collected from the investigated granitoids for the purpose of petrographic, geochemical, isotopic characterization, and age determination. Zircon concentrates were separated from six samples, about 20 kg each. Standard polished thin-sections were prepared for petrographic study at the Department of Geology, the University of Jordan; and for microprobe analysis at Helmholtz-Zentrum Potsam, Deutsches GeoForschungsZentrum (GFZ) laboratories in Potsdam and at the Institute for Mineralogy and Crystallography, Stuttgart University, Germany. Sample powder preparation for chemical analysis was also carried out at the University of Jordan and GFZ.

Bulk chemistry was determined at the GFZ, namely H_2O and CO_2 on elementary analyzer (Vario EL); major oxides and selected trace elements (Ba, Cr, Ga, Ni, Nb, Rb, Sr, V, Zn, and Zr) on Axios advanced spectrometer system from Panalytical; the REE and Ba, Y, Li, Co, Cu, Zn, Rb, Sr, Cs, Nb, Hf, Ta, Pb,

Th, and U for 24 samples on Inductively coupled plasma-atomic emission spectrometer ICP-AES(VISTA MPX); and the concentrations of Li, Be, Nb, Mo, Cd, Cu, Tl, Bi, Co, Sb, and Sn were determined on the VG Plasma Quad PG2 ICP-MS following the procedure outlined by Romer and Hanhe (2010). Details on the procedure of REE concentration and analysis can be found in Zugeler and Erzinger (1988) and Dulski (2001).

A total of 52 zircon, 12 titanite, and 6 feldspar fractions were separated from six whole rock samples at the GFZ geochronology lab in Potsdam. Jaw and roller crusher were utilized for grinding the samples to less than 400-micron size. The concentration of zircons, titanite, and feldspar was achieved using shaking table, heavy liquids: bromoform and di-iodomethane, and a Frantz magnetic Barrier separator (LB-1). Additional purification was performed by hand-picking under a binocular microscope. The zircons of Feinan and Mubarak granites were further abraded by pyrite in a small metallic instrument that uses air pressure to remove coated and weathered rims. Purified zircons and titanites were cleaned by washing successively with 7N HNO3, distilled water, and acetone. Thereafter, ca. 0.1 mg fractions were prepared, spiked with ^{205}Pb-^{235}U tracer, and dissolved in concentrated HF in a Parr autoclave for four days at 200 °C; dried and redissolved in 6N HCl for one day at 200 °C. Three to 4 mg of feldspar from each sample were ground in a mortar and leached with a mixture of 0.8N HBr and HF to get rid of non-structural lead. The cleaned feldspar was then dissolved in HF on a hotplate at ca. 160 °C overnight. For whole rock Rb-Sr and Sm-Nd isotopic analysis, ca 140 mg of powdered rock were dissolved in HF for four days at 160 ◦C and redissolved in 6N HCl for one day (Pfaff et al., 2009). Extraction of U, Pb, Sr, and Nd from zircons, titanite, feldspar, and whole rock samples was performed using ion exchange chromatography described by Schmidt et al., 2003; Pfaff et al., 2009; and Romer and Hahne, 2010. Lead and uranium were loaded together with HNO3 and silica gel on single rhenium filaments and their isotopic composition was measured at 1210-1240 and 1320-1420 ◦C, respectively on Finnigan MAT262 multicollector mass spectrometer in static multicollection mode. Mass fractionation was corrected with 0.1% / amu.(Pfaff et al., 2009). Strontium was loaded on a single Ta-filament and its isotopic composition was measured on a TRITON multicollector mass spectrometer in a dynamic multi-collection setup; while neodymium was loaded on a double Re-filament and its isotopic composition was measured on a Finnigan MAT262 multicollector mass spectrometer.

5. Geochemistry

The chemical data, including CIPW norms for the studies rocks, are listed in Table 1 (supplementary data, available upon request from the third author). The investigated granitoids have average silica contents of 76.3, 74.5, 76.7, and 65.3 wt. % for the Humrat, Feinan, Mubarak, and Sabil, respectively. On the Harker variation plots (Figure. 7) of selected major and trace elements versus silica, the four units define a smooth liquid line of descent starting with the Sabil granodiorite and ending with Humrat granite. Nevertheless, the Humrat, Mubarak, and Feinan lithologies do show cluster of data points rather than a scatter and this is due to their narrow range of silica content.

Article in Press: JJEES 16(2), June 2025.
This article has been accepted for publication and will appear in the upcoming issue. The final published version will be available through the journal website after copyediting, typesetting and proofreading. ©2025 JJEES.

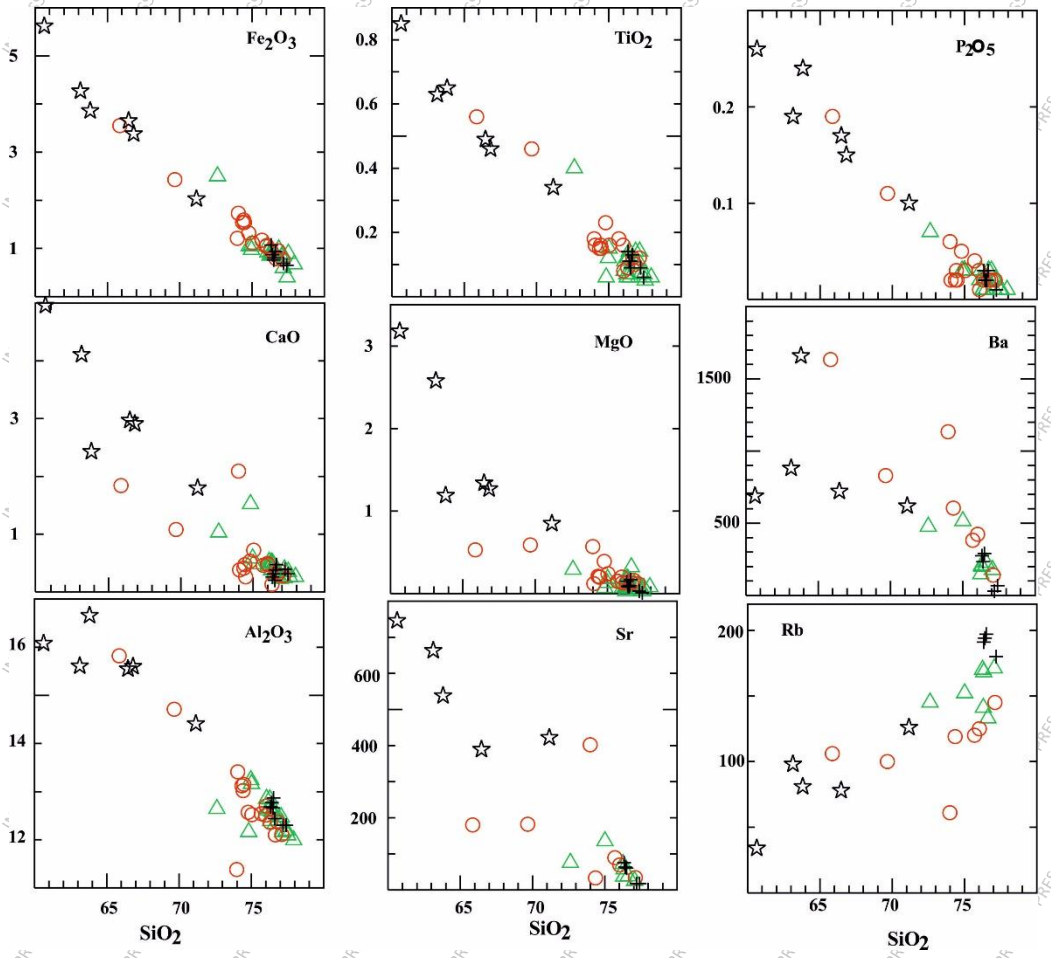

Figure. 7. Harker variation diagrams of major elements (wt.%), Rb, and Sr (ppm) versus silica (wt.%) of the investigated rock units. Symbols: Stars = Sabil granodiorite, circles = Feinan granite, triangles = Humrat granite, crosses = Mubarak

The normative mineralogy places the first three rock units (HFM) into the syeno- to alkali-feldspar granite fields and the Sabil unit into and quartz monzodiorite and granodiorite fields (Figure. 8A). Furthermore, the Humrat-Feinan-Mubarak (HFM) alkali feldspar granite cluster close to the granite minimum on the normative AB-Q-OR triangle while Sabil samples plot further down from this point together with two samples from the Feinan granite (Figure. 8B). Most of the samples of the HFM samples plot in the field of A-type granite except for few samples that straddle the border to the I and S-type granites (Figure. 8C). On the same plot the Sabil samples fall into the I and S-type granites or close to the border to the A-type field. The investigated two suites belong to the high-K alkali-calcic to alkali granitoids (Figure 8D & E). The HFM granites have a ferroan affinity while the Sabil unit granodiorites is magnesian in the sense of Frost et al. 2001 (Figure. 8F). Furthermore, the majority of the samples plot in the peraluminous field (Figure. 8G).

Article in Press: JJEES 16(2), June 2025.
This article has been accepted for publication and will appear in the upcoming issue. The final published version will be available through the journal website after copyediting, typesetting and proofreading. ©2025 JJEES.

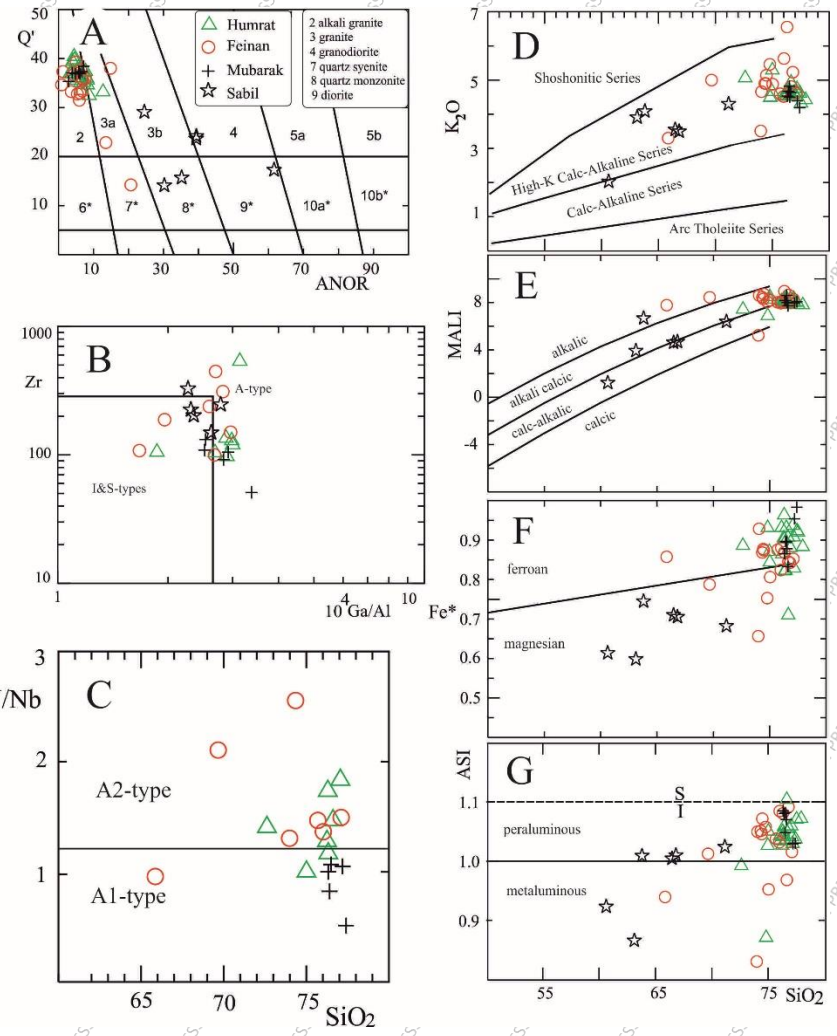

Figure. 8. Chemical classification diagrams of the investigated rocks. **A**. Q'-ANOR normative classification of igneous rocks (Streckeisen and Le Maitre, 1979), **B.** Zr (ppm)-(10000*Ga/Al) classification of granitoids (Whalen et al., 1987).

C. Y/Nb vs. SiO2 (wt. %) discrimination diagram of A-type granites (Eby, 1992), **D**. K2O (wt.%) vs. SiO2 (wt. %) plot with lines after LeMaitre 1989 and Rickwood 1989, E. MALLI Index vs. SiO2 (wt.%) (Frost and Frost, 2008), **F.** Fe-index vs. SiO2 (wt. %) (Frost et al., 2001), **G.** ASI (Alumina saturation index) vs. SiO2 (wt. %) (Frost et al., 2008)

The investigated granitoids display three different chondrite-normalized patterns: The Humrat and Feinan have almost identical patterns with enriched LREE patterns and flat HREE and strong Eu anomaly (Figure. 9A & B); the Mubarak granites, on the other hand, shows a concave upward pattern with the lowest total REE content (Fig. 9C); To the contrary, the Sabil granodiorite (Figure. 9D) have a steep pattern (La/Lu)N = 8.4-25.5 with weak negative anomaly (Eu/Eu*=0.7-1.0) . The Dy/Dy* was calculated using the formula suggested by Davidson et al., 2013 and plotted versus Dy/Yb ratios. The well-defined trend on this diagram (Figure. 10) points to amphibole and clinopyroxene fractionation as controlling factor in the evolution of these granitoids where the Mubarak granites suffered the highest degree of differentiation

Article in Press: JJEES 16(2), June 2025.
This article has been accepted for publication and will appear in the upcoming issue. The final published version will be available through the journal website after copyediting, typesetting and proofreading. ©2025 JJEES.

Figure. 9. Chondrite-normalized pattern for the Humrat (A), Feinan (B), Mubarak (C), Sabil (D) units, respectively. Normalizing values are from Sun and McDonough, 1989.

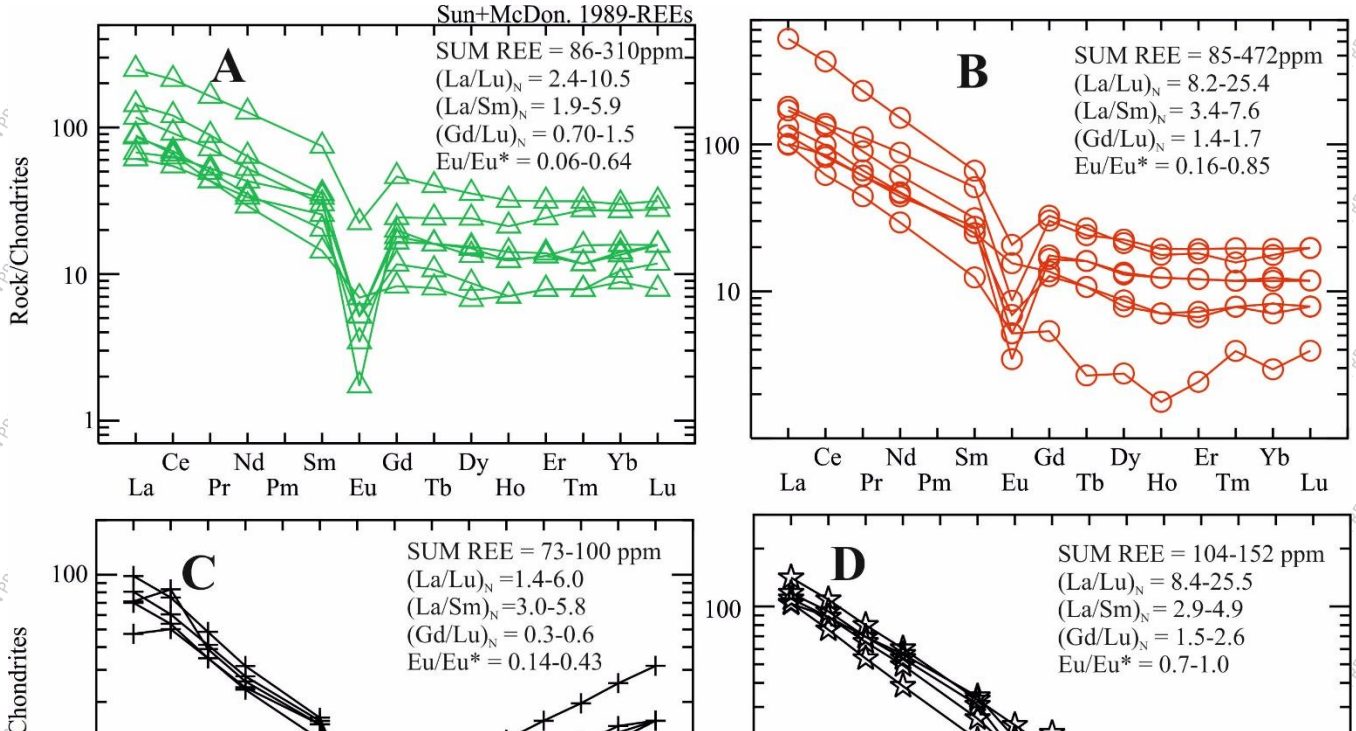

Article in Press: JJEES 16(2), June 2025.
This article has been accepted for publication and will appear in the upcoming issue. The final published version will be available through the journal website after copyediting, typesetting and proofreading. ©2025 JJEES.

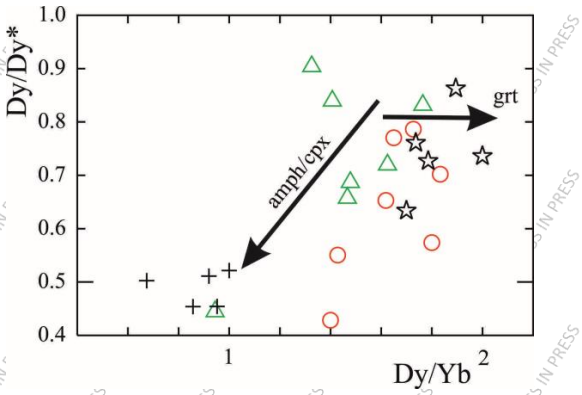

Figure. 10. The Dy/Dy* vs. Dy/Yb plot (Davidson et al., 2013). The arrow indicated by the garnet might indicate the amount of residual garnet in the source area of Sabil granodiorite.

On the multi-element spider diagram, the HFM (Figure. 11A, B, and C) as well as the Sabil (Figure. 11D) units are variably enriched in Cs, Rb, Th, U, and Pb. On the other hand, the HFM units display variable degrees of Ba, Sr, and P depletions with Mubarak being the most prominent. The strongest Nb-Ta anomaly is shown by the Sabil unit and followed by Feinan, Humrat, and Mubarak in a decreasing order.

Article in Press: JJEES 16(2), June 2025.
This article has been accepted for publication and will appear in the upcoming issue. The final published version will be available through the journal website after copyediting, typesetting and proofreading. ©2025 JJEES.

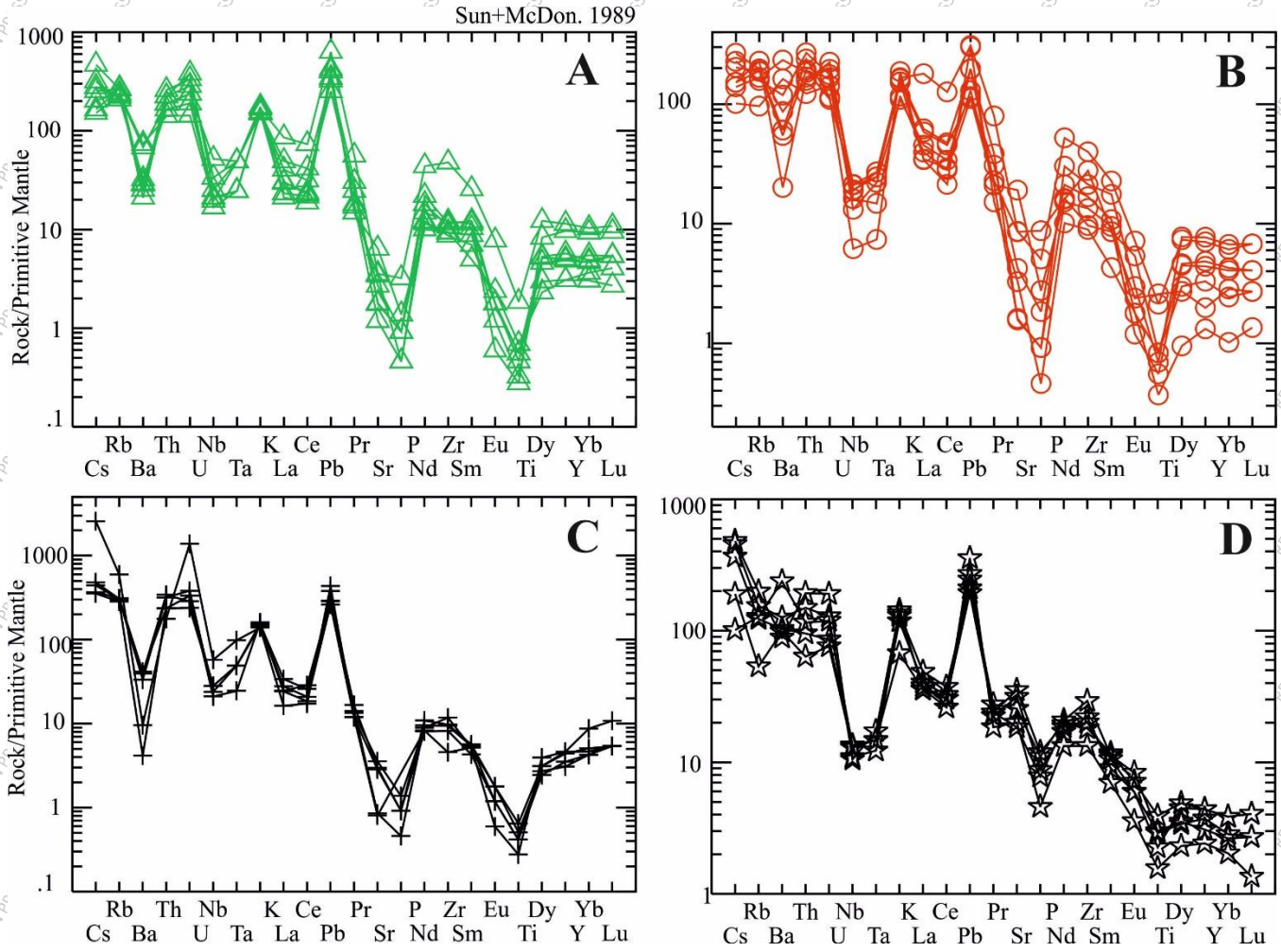

Figure. 11. Multi-element spider diagrams for the Humrat (A), Feinan (B), Mubarak (C), and Sabil (D) units, respectively.

The trace element data is further used to make inferences regarding the tectonic setting of the investigated rocks and to discriminate the A-type granite. On the Nb-Y diagram (Figure 12A, Pearce et al. 1984) all samples plot in the VAG and syn-collisional granite except for 2 samples from Humrat and one from Mubarak units which fall in the within plate field. On the Rb versus Nb+Y diagram (Figure. 12 B, Pearce et al. 1984; Pearce et al. 1996) almost all samples plot in the post-collisional field. The post-collisional setting for the Humrat and Mubarak units is further confirmed by the Hf-Rb/30- Ta*3 and Hf-Rb/30-Nb/4 ternary plots (Figure. 12 C & D, Harris et al. 1986). On the other hand, the Feinan and Sabil units fall into the VAG field. The within-plate setting for the HFM units is confirmed by the Nb/Y vs. SiO2 diagram (Figure. 12 E, Pearce and Gale, 1977). Nonetheless, two samples from Feinan Unit plots together with the samples from the Sabil unit in the field of volcanic arc magmas.

Article in Press: JJEES 16(2), June 2025.
This article has been accepted for publication and will appear in the upcoming issue. The final published version will be available through the journal website after copyediting, typesetting and proofreading. ©2025 JJEES.

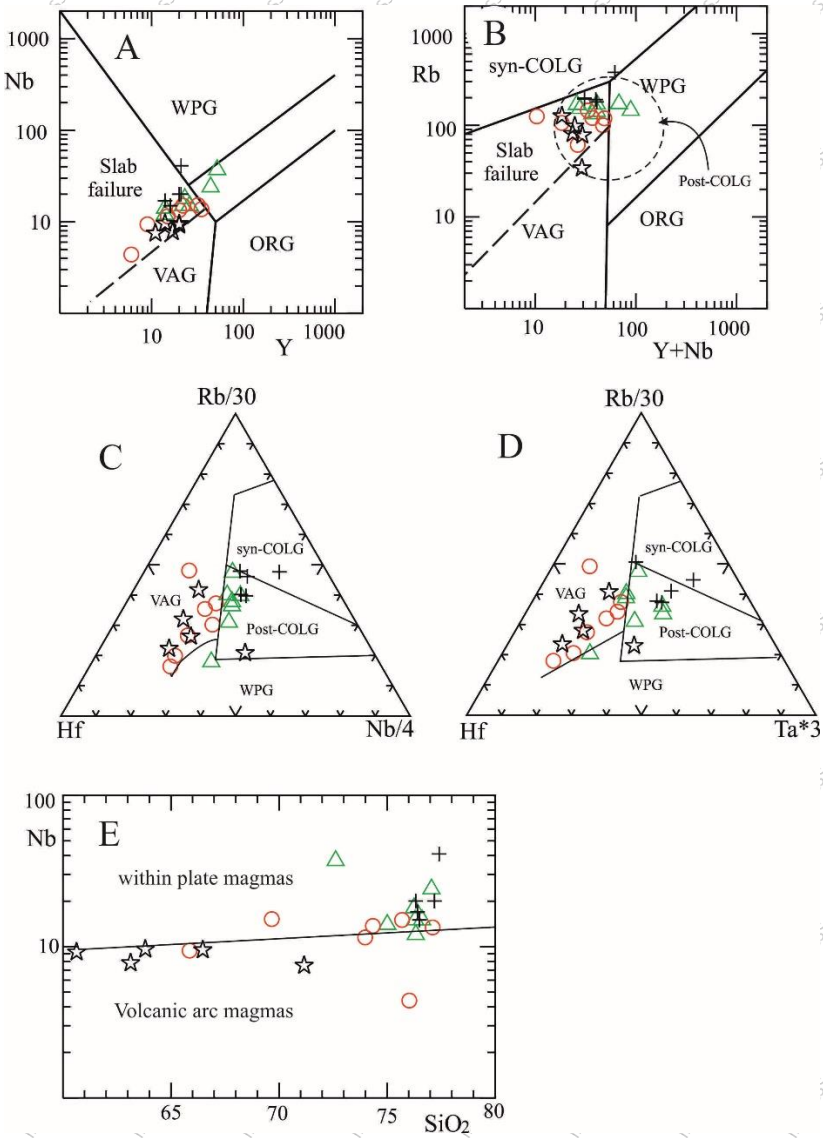

Figure. 12. Tectonic discrimination diagrams.

A. Nb (ppm) vs. Y (ppm) (Pearce et al. 1984), **B**. Rb (ppm) vs. Y+Nb (ppm)(Pearce et al. 1996), **C** & **D**. Hf-Rb-Ta (ppm) plots after Harris et al. 1986, **E**. Nb (ppm) vs SiO2 (wt. %) (Pearce and Gale, 1977). Symbols as in Figure. 7. The dashed line in A and B separates the volcanic arc granite (VAG) from Slab failure granites in the sense of Whalen and Hildebrandt (2019).

6. Mineral chemistry and thermo-barometric constraints.

Four representative polished thin sections (NF-8, NF-31, NF- 39, and NF-43) were made from the four investigated units and analyzed for plagioclase, alkali feldspar, amphibole, biotite, and opaques on Cameca electron microprobe (SX-100) at the Institute for Mineralogy and Crystallography, University of Stuttgart, Germany. Representative analyses with their respective chemical formulae are presented in Appendix 2. The feldspar chemical variation of the four units is shown in Figure 13A. In the granitic unit of Feinan, Humrat, and Mubarak, the alkali feldspars are either anorthoclase ($Or_{0\text{-}30\,\%}$) or orthoclase ($Or_{70\text{-}100\%}$). On the other hand, they are K-rich ($Or_{85\text{-}95\%}$) in the Sabil granodiorite unit.

The orthoclase of the Sabil (Sabit) granodiorite is in equilibrium with oligoclase ($An_{10\text{-}30\,\%}$). The amphiboles of the Sabil granodiorite are classified as Edenites of the calcic-amphiboles (Figure. 13B). We used the Zr content of the investigated rocks vs. their chemistry expressed by the parameter M = (Na+K+2Ca)/(Al*Si) to estimate the temperature of crystallization. The Sabil granodiorites cluster between the isotherms 800 -850 C. Humrat and Mubarak granite mostly around 800 while the Feinan

Article in Press: JJEES 16(2), June 2025.
This article has been accepted for publication and will appear in the upcoming issue. The final published version will be available through the journal website after copyediting, typesetting and proofreading. ©2025 JJEES.

granites show a larger scatter 800 – 850. Nevertheless, two samples from the granites fall around 950C. Furthermore, the crystallization of the Sabil granodiorite was modeled using the online MELTS-software (Ghiorso et al., 2015). All modal minerals of these rocks appeared in the model in a sequence starting with oligoclase, followed by titanomagnetite, biotite, orthoclase, quartz, hornblende and ending with apatite, and titanite. Equilibration and sub-solidus reactions seem to have continued up to 600 °C (Figure.13. D). The order of crystallization and the amount of modeled minerals fits well with thin section observations (Figure. 6A&B).

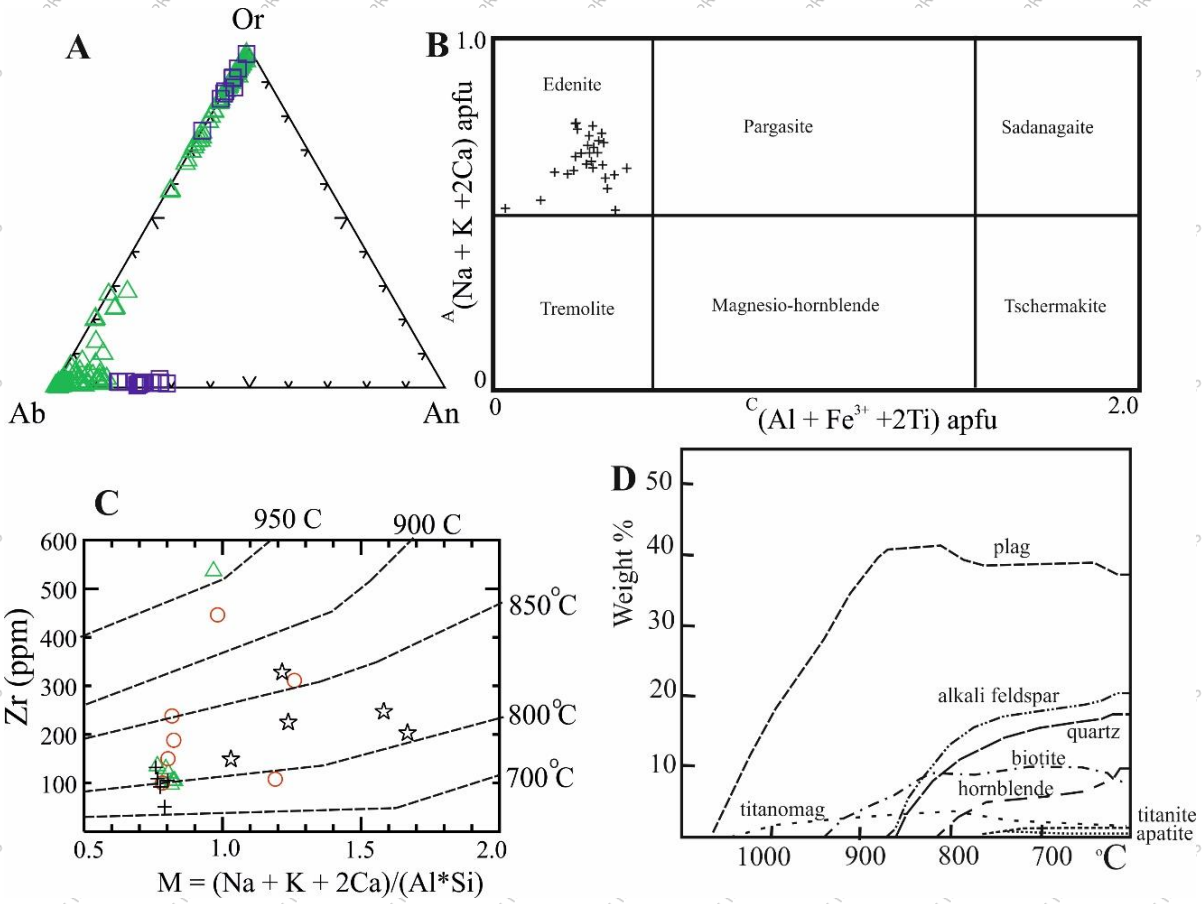

Figure. 13. A. Compositional variation of feldspars in the investigated rocks. The blue squares for Sabil granodiorites, **B**. Amphibole chemistry plotted on the calcic-amphiboles diagram (Hawthorne et al. 2012), C. Zircon saturation thermometer (Watson & Harrison, 1983), D. Crystallization sequence and amounts of minerals in the Sabil granodiorite modeled by MELTS-Software (Ghiorso and Gualda, 2015).

7. Geochronology

A total of fifty two euhedral to subhedral inclusions and fractures—free zircon fractions and twelve titanites fractions— were separated from bulk samples of the four investigated rock units. Turbid and partially metamict zircons were abraded to get clear fresh cores. The isotopic data is presented in Table 2 while the concordia plots for the investigated units are shown in Figure 13. The $^{207}Pb/^{206}Pb$ ages

Article in Press: JJEES 16(2), June 2025.
This article has been accepted for publication and will appear in the upcoming issue. The final published version will be available through the journal website after copyediting, typesetting and proofreading.

were calculated (Table 2), as these are insensitive to recent lead loss. Potassium feldspar was separated from the same samples and leached before analysis following the procedure by Romer, et al. (1996) and used for the correction of common Pb (Table 3).

A summary of the robust zircon U–Pb ages for all samples is discussed below.

Article in Press: JJEES 16(2), June 2025.
This article has been accepted for publication and will appear in the upcoming issue. The final published version will be available through the journal website after copyediting, typesetting and proofreading. ©2025 JJEES.

Table 2. The isotopic data of the investigated rocks.

Sample[a] (zircon fractions)		Weight (mg)	Concentration (ppm)		Measured ratios[b]	Radiogenic Pb (at.%)[c]				atomic ratios[c]			Apparent ages (Ma)[d]		
			U	Pb_{tot}	$^{206}Pb/^{204}Pb$	^{206}Pb	^{207}Pb	^{208}Pb	$^{238}U/^{204}Pb$	$^{206}Pb/^{238}U$	$^{207}Pb/^{235}U$	$^{207}Pb/^{206}Pb$	$^{206}Pb/^{238}U$	$^{207}Pb/^{235}U$	$^{207}Pb/^{206}Pb$
Humrat Alkali granite															
NF1 Zircon	1	0.048	480.4	34.06	534.792	6.120	0.35	0.68	8894	0.0636	0.4959	0.0565	398	409	474
	2	0.038	618.9	50.50	1115.58	7.260	0.44	1.19	17544	0.0741	0.6117	0.0599	461	485	599
	3	0.078	658.5	54.07	821.353	15.79	0.94	2.37	11504	0.0737	0.6049	0.0595	458	480	587
	4	0.120	923.4	65.69	657.905	29.02	1.73	4.27	10446	0.0628	0.5152	0.0595	393	422	586
	5	0.098	1084	85.34	979.601	31.97	1.89	4.36	13775	0.0721	0.5892	0.0593	449	470	576
	6	0.109	1093	81.39	471.150	31.65	1.88	4.50	7225	0.0637	0.5219	0.0594	398	426	583
	7	0.192	1057	79.87	603.624	55.90	3.35	8.28	8979	0.0660	0.5451	0.0599	412	442	600
NF11 Zircon	8	0.092	581.7	57.92	166.051	14.90	0.89	2.85	2243	0.0668	0.5481	0.0596	417	444	588
	9	0.084	550.8	46.15	531.101	13.54	0.80	2.61	7608	0.0702	0.5744	0.0594	437	461	581
	10	0.127	551.5	67.25	108.146	20.04	1.20	4.20	1323	0.0686	0.5660	0.0599	428	455	598
	11	0.096	506.0	48.98	194.460	13.72	0.81	2.71	2642	0.0677	0.5538	0.0593	422	448	578
	12	0.116	657.6	51.14	366.722	19.94	1.19	3.57	5671	0.0627	0.5126	0.0596	392	422	588
	13	0.134	549.2	51.12	298.805	22.16	1.32	4.11	3945	0.0722	0.5926	0.0596	449	473	587
Feinan Alkali granite															
NF21 Abraded zircon	14	0.085	335.4	31.36	1340.56	9.860	0.59	2.01	18496	0.0829	0.6859	0.0600	513	530	605
	15	0.113	377.1	34.80	1677.92	14.78	0.89	2.83	22691	0.0831	0.6886	0.0601	515	532	606
	16	0.091	448.2	42.06	952.87	13.96	0.84	2.74	12235	0.0821	0.6800	0.0601	509	527	607
	17	0.106	319.5	32.30	1075.35	12.62	0.76	2.42	12946	0.0894	0.7396	0.0603	552	562	604
	18	0.098	480	51.9	193	14.8	0.89	2.89	2347	0.0756	0.6288	0.0603	470	495	616
	19	0.171	448	48.2	330	26.9	1.62	5.21	3746	0.0843	0.6971	0.0600	522	537	604
NF21 Non abraded zircon	20	0.105	363	44.26	1813	17.65	1.06	3.19	18083	0.1111	0.9177	0.0599	679	661	601
	21	0.111	546	42.86	492	16.46	0.99	3.18	7518	0.0651	0.5370	0.0599	406	437	599
	22	0.099	388	37.5	650	13.11	0.79	2.67	8115	0.0819	0.6761	0.0599	509	524	600
Titanite	23	0.183	67.3	17.03	141.730	6.040	0.36	5.21	1074	0.1177	0.9742	0.0600	717	691	604
	24	0.201	73.3	16.24	110.500	5.730	0.34	5.31	1008	0.0934	0.7729	0.0600	576	581	605
	25	0.218	37.3	9.300	136.851	3.350	0.20	4.29	1248	0.0989	0.8201	0.0602	608	608	610
	26	0.284	92.4	18.39	146.938	11.11	0.67	7.35	1287	0.1015	0.8447	0.0604	623	622	616
	27	0.181	76.6	36.14	39.0540	6.060	0.36	4.72	203	0.1048	0.8498	0.0588	642	625	560
	28	0.249	60.6	13.52	143.412	6.430	0.38	5.84	1253	0.1022	0.8367	0.0594	627	617	581
NF31 Abraded zircon (1st time)	29	0.094	1025.3	93.650	744.366	32.60	1.95	4.94	9170	0.0811	0.6703	0.0599	503	521	601
	30	0.083	917.50	86.220	579.161	26.25	1.58	3.56	6944	0.0827	0.6851	0.0601	512	530	608
	31	0.076	1115.4	105.98	447.262	28.40	1.69	4.15	5408	0.0803	0.6593	0.0598	498	514	597
	32	0.130	1026.6	97.060	639.762	46.34	2.79	6.73	7582	0.0832	0.6919	0.0603	516	534	614
	33	0.243	1113.0	104.70	406.150	88.61	5.30	13.0	4968	0.0786	0.6476	0.0598	487	507	596
	34	0.121	1314.9	120.05	524.693	52.43	3.14	7.45	6483	0.0790	0.6530	0.0599	490	510	602

Article in Press: JJEES 16(2), June 2025.
This article has been accepted for publication and will appear in the upcoming issue. The final published version will be available through the journal website after copyediting, typesetting and proofreading. ©2025 JJEES.

NF31	35	0.099	1858.5	186.11	2271.76	72.05	4.32	10.7	24820	0.0939	0.7767	0.0600	578	584	604
Abraded zircon (2^{nd} time)	36	0.099	1581.1	159.82	1152.80	59.84	3.59	9.5	12629	0.0917	0.7582	0.0600	565	573	603
	37	0.084	1747.3	179.99	1141.55	57.59	3.45	8.6	12191	0.0941	0.7780	0.5997	580	584	603
	38	0.106	1906.8	191.86	1445.04	78.28	4.70	11.7	15683	0.0928	0.7679	0.0600	572	579	603
	39	0.188	1636.5	163.17	1796.50	119.1	7.14	17.8	19503	0.0928	0.7673	0.0600	572	578	603
	40	0.199	1855.6	186.51	1301.10	140.8	8.45	22.8	14182	0.0914	0.7565	0.0600	564	572	604
NF31	41	0.099	1145.4	111.35	386.538	38.13	2.28	5.63	4619	0.0806	0.6633	0.0597	500	517	592
Non abraded zircon	42	0.085	1576.9	157.50	390.598	46.04	2.76	7.24	4564	0.0824	0.6805	0.0599	510	527	601
Mubarak Alkali granite															
NF38	43	0.076	557.4	59.67	713.435	16.76	1.01	2.55	7660	0.0949	0.7846	0.0600	584	588	603
Abraded zircon	44	0.121	570.3	68.28	278.435	27.01	1.62	4.01	2806	0.0938	0.7749	0.0599	578	583	600
	45	0.080	564.6	62.97	438.074	17.51	1.05	2.92	4635	0.0929	0.7680	0.0599	573	579	601
	46	0.071	637.4	71.93	403.645	17.64	1.06	2.82	4222	0.0935	0.7722	0.0599	576	581	600
	47	0.101	437.5	48.18	430.529	17.03	1.02	2.63	4580	0.0924	0.7634	0.0599	570	576	601
	48	0.186	597.5	67.75	367.443	43.28	2.61	6.33	3777	0.0934	0.7764	0.0603	575	583	615
	49	0.070	772	96.90	204.078	20.55	1.23	3.20	2062	0.0912	0.7548	0.0600	562	571	605
NF38	50	0.080	853.1	96.75	324.809	26.23	1.58	3.61	3372	0.0921	0.7653	0.0602	568	577	612
Non abraded zircon	51	0.160	827.4	96.66	262.988	49.41	2.98	8.09	2754	0.0895	0.7430	0.0602	553	564	611
	52	0.096	704.2	76.47	316.610	24.27	1.46	4.05	3515	0.0861	0.7150	0.0602	532	548	612
	53	0.105	712.7	84.75	234.954	27.66	1.67	4.67	2470	0.0886	0.7363	0.0603	547	560	613
Sabil granodiorite															
NF8 Zircon	54	0.099	236.4	25.91	2829.989	9.65	0.58	2.03	40628	0.0988	0.8205	0.0602	608	608	611
	55	0.130	252.2	26.65	3969.613	13.33	0.81	2.49	59367	0.0975	0.8112	0.0604	600	603	617
	56	0.104	255.1	27.66	4878.034	10.96	0.66	2.22	90078	0.0991	0.8263	0.0605	609	612	621
	57	0.089	268.7	28.74	2768.216	9.71	0.59	1.91	39789	0.0974	0.8093	0.0603	599	602	614
	58	0.105	230	24.31	4559.555	9.83	0.59	1.86	88324	0.0976	0.8123	0.0604	600	604	616
	59	0.153	183.2	19.58	1547.832	11.26	0.68	2.12	18644	0.0963	0.8014	0.0603	593	598	616
NF8 Titanite	60	0.168	229.2	42.77	545.914	17.66	1.09	13.65	4958	0.1099	0.9381	0.0619	672	672	671
	61	0.203	223.5	43.85	446.517	20.04	1.21	18.47	4139	0.1059	0.8790	0.0602	649	640	611
	62	0.253	213.7	41.64	538.095	23.72	1.43	22.54	5062	0.1051	0.8728	0.0602	645	637	611
	63	0.244	216.1	46	485.418	23.75	1.44	25.44	4419	0.1080	0.9007	0.0605	661	652	621
	64	0.236	173.5	40.18	591.450	19.96	1.21	22.19	5057	0.1169	0.9742	0.0605	713	691	620
	65	0.182	188.2	40.87	618.905	16.04	0.97	17.07	5566	0.1123	0.9335	0.0603	686	670	614

[a] Zircon concentrates were cleaned in warm 7N HNO_3 and H_2O before dissolution in concentrated HF in teflon-lined autoclaves at 210°C for 4 days. A mixed ^{205}Pb-^{235}U tracer was added before sample dissolution. Lead and U were separated using ion-exchange chromatographic procedures (e.g., ROMER et al., 1996; SCHMID et al., 2003). Lead and U were loaded together on single Re-filaments using a silica-gel emitter and H_3PO_4 (GERSTENBERGER & HAASE, 1997) and measured at 1200°–1260°C and 1350–1400°C, respectively, on a Finnigan MAT262 multicollector mass-spectrometer (modified with an ion source by Spectromat) using Faraday collectors and ion counting.

[b] Lead isotope ratios corrected for fractionation (0.1% / a.m.u.).

[c] Lead corrected for fractionation, blank, tracer contribution, and initial lead ($^{206}Pb/^{204}Pb$ = 18.1±0.1, $^{207}Pb/^{204}Pb$ = 15.60±0.02, $^{208}Pb/^{204}Pb$ = 38.2±0.2). During the measurement period, total blanks were <15 pg for lead and <1 pg for uranium.

[d] Apparent ages were calculated using the constants recommended by IUGS (STEIGER & JÄGER, 1977).

Article in Press: JJEES 16(2), June 2025.
This article has been accepted for publication and will appear in the upcoming issue. The final published version will be available through the journal website after copyediting, typesetting and proofreading.

7.1. Sabil granodiorite unit (NF8)

The uranium and lead contents of the zircons of this unit range between 183 – 269 ppm and 20 – 29 ppm, respectively. They have the highest measured $^{206}Pb/^{204}Pb$ ratios (Table 3) due to their very low common Pb content (0.16 – 0.61 ppm). The data points defined a cluster of concordant to sub-concordant data points on the Terra – Wasserburg Concordia diagram. Nevertheless, the clustering of the data does not constrain a discordia. The U-Pb zircon age is calculated in two ways: (i) A discordia is fitted through the origin of the diagram (0 ± 50 Ma). This yields an upper intercept of 615.8 ± 1.9 Ma (2σ; MSWD = 1.9) (Figure. 14 A). Although six zircon analyzed fractions have been used to calculate the discordia, this analysis essentially represents a two-point discordia (i.e., the data cluster and the origin of the diagram). It should be mentioned here that, without forcing the discordia to pass through zero, the age is 614.3 ± 4.2 M which agrees with the titanite age (614.1 ± 4.2 Ma). The major effect of forcing the discordia through the origin is to increase the age slightly and to reduce the error and the MSWD to more precise values (±1.9 Ma; MSWD = 1.9).
(ii) The weighted $^{207}Pb/^{206}$ Pb age is 615.8 ± 2.7 Ma (2σ, MSWD = 1.9). Both ways to calculate the age implicitly assume a recent disturbance of the U-Pb systems. This assumption has been used to interpret the Discordia diagrams obtained using conventional U-Pb zircon dating of the granitoids in the Arabian-Nubian Shield (e.g. Jarrar et al., 1983; Pallister et al., 1988). The titanite obtained from this sample has a high common lead content (2.1 -3.24 ppm) and, as a result, low to moderate $^{206}Pb/^{204}Pb$ ratios. The data points of these titanites are up to 30% discordant and fall above Concordia diagram; therefore, they are not discussed further. The age of 615 Ma has also been obtained for the same gabbro using single zircon dating (Ben Sireh, 2018, unpublished PhD thesis).

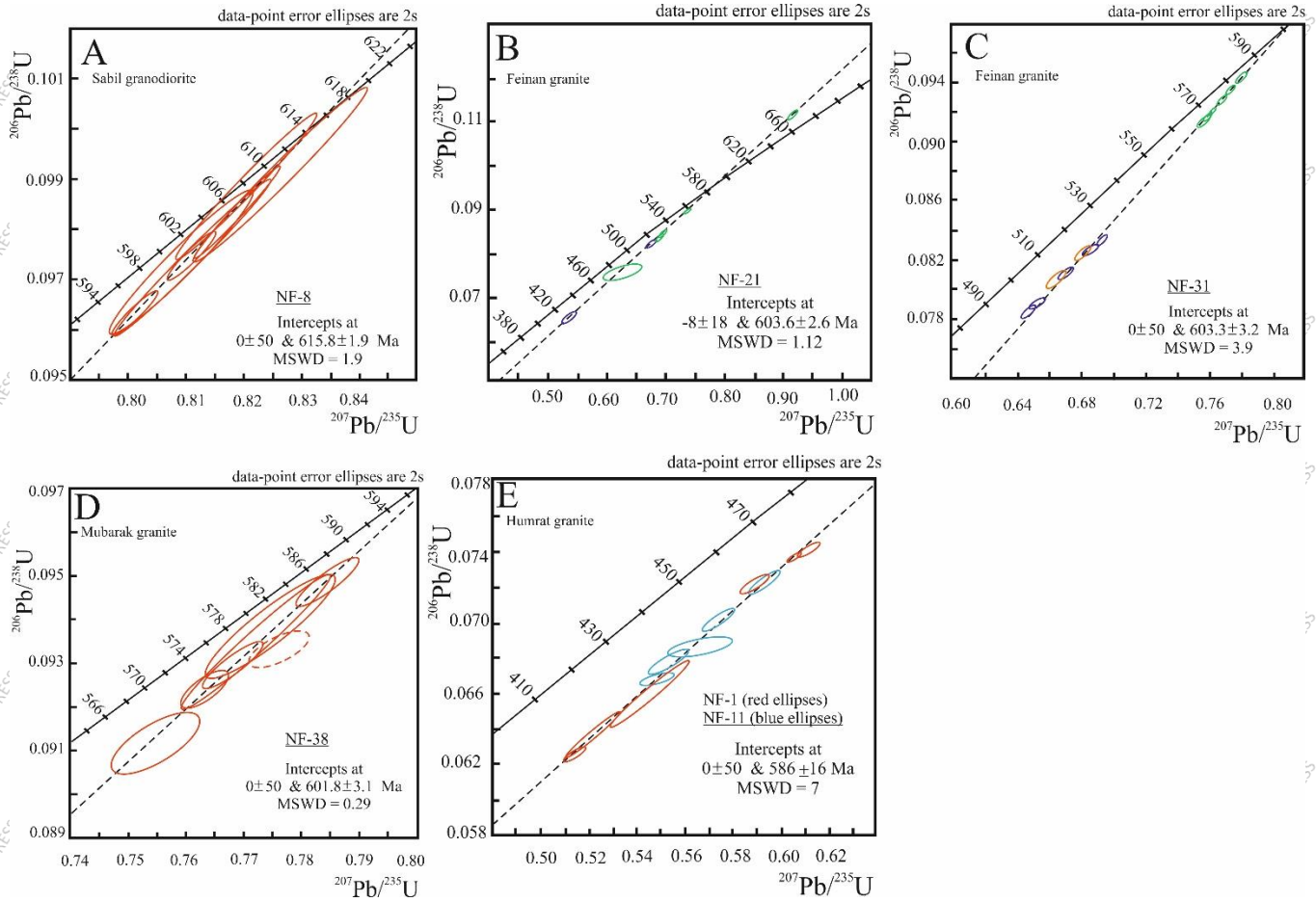

Article in Press: JJEES 16(2), June 2025.
This article has been accepted for publication and will appear in the upcoming issue. The final published version will be available through the journal website after copyediting, typesetting and proofreading. ©2025 JJEES.

Figure. 14. Zircon and titanite Concordia diagrams of the studied rocks.

7.2. Feinan alkali granite (NF21 & NF31)

A twenty-two zircon fractions and titanite grains were hand-picked from NF21 and NF31 samples from the Feinan Alkali granite.

7.2.1 NF21 Zircons

Two zircon fractions have 388 and 546 ppm of uranium and 38 and 43 ppm of total lead with low measured $^{206}Pb/^{204}Pb$ ratios (Table 3) and high common lead content of 3 and 4.5 ppm, respectively. Six more fractions of abraded zircon contain less uranium and total lead, about 320 – 448 ppm and 31–48 ppm, respectively, along with higher measured $^{206}Pb/^{204}Pb$ ratios (Table 3) compared to the non-abraded zircon fractions. The common Pb content is low; around one ppm for all samples except for fraction 18 that contains 7 ppm (Table 3). This indicates that abrasion preferentially removed metamict domains, which in addition to a disturbed U-Pb system also have higher contents of common Pb.

All the samples are discordant and close to the upper intercept, where the non -abraded samples are more discordant and scattered reflecting lead loss. Although few, they yield lower and upper intercepts of 6 ± 46 and 601 ± 11 Ma (2σ; MSWD = 0.0), whereas the abraded samples are less discordant and close to the intercept. They define a line with lower and upper intercepts of -20 ± 21 and 602.6 ± 2.8 Ma (2σ; MSWD = 0.25), consistent with the non-abraded ones. Thus, both abraded and non-abraded samples were plotted together and yielded a discordia line intercepting the Concordia at a more reliable and precise intercept of 603.6 ± 2.6 Ma (2σ; MSWD = 1.12) (Figure. 14B). Titanites are highly heterogeneous and produced intercepts with high uncertainty and therefore are not considered further.

Table 3. Initial Pb isotope data and preferred zircon ages of the investigated granitoids of south Jordan.

Sample	Preferred Zircon age (Ma)	$\frac{^{206}Pb}{^{204}Pb}$ a	$\frac{^{207}Pb}{^{204}Pb}$ a	$\frac{^{208}Pb}{^{204}Pb}$ a
Humrat Alkali granite				
NF1	587±17	17.807	15.570	37.534
NF11	584±16	17.860	15.572	37.581
NF1 & NF11	586±16			
Mubarak Alkali granite				
NF38	601.8±3.1	17.973	15.565	37.561
Feinan Alkali granite				
NF21	603.6±2.6	17.728	15.540	37.426
NF31	603.3±3.2	17.700	15.552	37.488
Sabil Granodiorite				
NF8	615.8±1.9	17.755	15.570	37.550
Average initial lead		17.804±0.3	15.562±0.05	37.523±0.5

Article in Press: JJEES 16(2), June 2025.
This article has been accepted for publication and will appear in the upcoming issue. The final published version will be available through the journal website after copyediting, typesetting and proofreading.

a. 3-4 mg of feldspar grains from each sample were smashed in the hand agate mortar, washed with water and a mixture of 0.8N HBr and HF were added to the samples to remove all radiogenic lead. Finally, they were put on a 160 °C hotplate overnight after adding HF to them (Romer and Hanhe, 2010) and measured at 1200 - 1260 °C and 1350 - 1400 °C, respectively, on a Finnigan MAT262 multicollector mass-spectrometer (modified with an ion source by Spectromat) using Faraday collectors and ion counting. Lead isotope data corrected for mass discrimination with 0.1 % / A.M.U. Reproducibility at 2σ level is better than 0.1 %.

7.2.2 NF31-Zircons

The non-abraded zircon fractions have high uranium content (1145 and 1577 ppm) and high total lead amount (111 and 158 ppm) with low measured $^{206}Pb/^{204}Pb$ ratios due to the too-high common lead (15 and 22 ppm). After the first abrasion of six fractions, their U content remains high while the total Pb decreases to (86 – 120 ppm) and the common lead decreases to (7–14 ppm), which increases the measured $^{206}Pb/^{204}Pb$ ratios. More intense abrasion of zircon increased the uranium and the lead to about (1581 – 1907 ppm) and (160 – 192 ppm), respectively. The drop in common lead (5 – 9 ppm) resulted in the high measured $^{206}Pb/^{204}$ Pb ratios (1142 – 2272 ppm, Table 3). As a conclusion, abrasion removed the metamict domains. The increase of the U content is somewhat unexpected as normally domains with higher U content turn more metamict than domains with low contents and, thus, are preferentially removed during abrasion. As abrasion also reduced the common lead content, the measured $^{206}Pb/^{204}Pb$ ratios of the abraded samples were higher. The higher U contents in the abraded samples may indicate that the rims of zircon had lower U contents than the cores did.
Plotting all data of this unit on the Concordia diagram shows that the non-abraded and slightly abraded samples are highly discordant, while the strongly abraded fractions are less discordant. The data of both abraded groups fall along a discordia line that intercepts the concordia at 5 ± 46 and 604 ± 5.3 Ma (2σ; MSWD = 3.4). Forcing the discordia through the origin of the diagram (0±50 Ma) does not affect the upper intercept significantly (603.4 ± 3.1 Ma, 2σ; MSWD = 3.2).
The discordia, produced from all data forced through the origin of the diagram, yields an intercept of 603.3 ± 3.2 Ma (2σ; MSWD = 3.9; Figure. 14C). Using all the layers here offers large spread (scatters) and doesn't affect the intercept age, but makes the line better defined (Figure. 14C). The average weighted $^{207}Pb/^{206}Pb$ age, also yields an age of 603.2 ± 1.6 Ma (2σ; MSWD = 3.8) indicating the robustness of this crystallization age.

7.3.Mubarak alkali granite (NF38)

The abraded zircons from sample NF38 contain 438 to 772 ppm U and a total of 48 to 97 ppm lead, respectively (Table 3). They are characterized by low measured radiogenic $^{206}Pb/^{204}Pb$ ratios which reflect the relatively high common lead content which varies from 4.5 to 23.3 ppm. The non-abraded fractions have higher uranium contents (704 – 853 ppm), and higher common lead contents (12.5–18.7) and consequently lower measured $^{206}Pb/^{204}Pb$ ratios.
All the samples are normally discordant and close to the upper intercept, where the abraded samples are slightly less discordant. As the data cluster, the slope of discordia is not well defined, although there is no or only little excess scatters, e. g., all the data have MSWD of 2.1. Omission of one abraded sample even reduced the MSWD to 0.29 (Figure. 14D).
Because of the close clustering of the data, the slope of the discordia is not well constrained and the intercept with the Concordia is flat, which yields a large uncertainty. Forcing the discordia for

Article in Press: JJEES 16(2), June 2025.
This article has been accepted for publication and will appear in the upcoming issue. The final published version will be available through the journal website after copyediting, typesetting and proofreading.

the abraded samples through the origin reduces the intercept to 601.8 ± 3.1 Ma with (2σ; MSWD = 0.29; Figure. 13D), which is congruent with the average weighted $^{207}Pb/^{206}Pb$ age (601.8 ± 2.4 Ma, 2σ; MSWD = 0.3), and illustrates the robustness of the age for this unit.

7.4.Humrat alkali feldspar granite unit

NF1 & NF11 - Zircons

The zircon from sample NF1 has U contents ranging from 480 to 1093 ppm and a total lead from 34 to 85 ppm (Table 3) with relatively high common lead content varying from 2.2 to 9.4 ppm, which caused low measured radiogenic $^{206}Pb/^{204}Pb$ ratios. As shown in Figure (6-6), the samples are scattering largely along the discordia (MSWD = 14), where zircons from sample NF11 have perfect dispersion beside them (MSWD = 0.78) (Figure 6-7), and contain about 506 – 582 ppm of U and 46–67 ppm of total lead. The same as NF1, due to the rather high content of common lead of 4.5–26 ppm, the measured $^{206}Pb/^{204}Pb$ is not very radiogenic.

Forcing the discordia through the origin of the diagram (0 ± 50) yields upper intercept age of 587 ± 17 and 584 ± 16 Ma for samples NF1 and N11, respectively. The large uncertainty of the upper intercept age is due to the highly discordant nature of the analyzed zircons and the small spread of the data points along the Concordia. The obtained upper intercept ages, however, are mostly identical.

Since the two samples of the Humrat Alkali unit (NF1 and 11) are from the same pluton and the zircons of both samples are highly discordant and show a relatively small range of scatter along the discordia, their ratios were plotted together on the concordia diagram and gave an age of 586 ± 16 Ma with a relatively high MSWD value equals to 7 (Figure. 14E) consistent with the average weighted $^{207}Pb/^{206}Pb$ age of 586.2 ± 5 Ma (2σ; MSWD = 7.1). A biotite rhyolite dike (600 ± 4 Ma, $^{40}Ar/^{39}Ar$ age of biotite), an andesite dike (594 ± 3, $^{40}Ar/^{39}Ar$ age of amphibole) and a dolerite dike (~579 Ma, 40Ar/39Ar whole rock total gas age) (Ghanem et al. 2020). The rhyolite and andesite dikes do not cut the Humrat granite, while the dolerite dikes are the only dikes cut through this granite elsewhere in the basement complex of south Jordan.

7.5 Rb-Sr and Sm-Nd data

Rb–Sr and Sm–Nd isotopic data are given in Table 4. Rb contents are higher than Sr contents in all samples except for the samples of the Sabil granodiorite Unit, with a maximum value of 22 in Mubarak Unit and a minimum value of 0.046 in the Sabil Unit (Table 1). This has great effects, in particular for weathered feldspars, on the $^{87}Sr/^{86}Sr$ ratios (Stoeser and Frost, 2006; Eyal et al., 2010). Therefore, only samples with $^{87}Rb/^{86}Sr$ ratios less than 4 were calculated for their initials because these should have experienced modest radiogenic growth for their $^{87}Rb/^{86}Sr$ (Stoeser and Frost, 2006). They yield initial $^{87}Sr/^{86}Sr$ ratios in the range from 0.70146 to 0.71508, with ascending averages of 0.70374, 0.70647, 0.70873, and 0.70947, for the Sabil, Feinan, Humrat and Mubarak samples, respectively. In particular, the high values (note these samples also have high εNd values) indicate that the Rb/Sr ratio is disturbed, which results in over-and under-correction of in situ ^{87}Sr growth. These values are close to the contemporary depleted mantle, since they are below the ratio of the granitic rocks that have been derived from the crust (0.729), as well as within and above the ratio of the basaltic magma (undifferentiated reservoir) which is 0.7045 (Faure and Mensing, 2005).

Article in Press: JJEES 16(2), June 2025.
This article has been accepted for publication and will appear in the upcoming issue. The final published version will be available through the journal website after copyediting, typesetting and proofreading.

The Nd and Sm contents of the granitoids range from 10.9 to 70.6 ppm and 1.87 to 11.4 ppm, respectively. The concentrations of these elements increase with increasing degree of differentiation, as in Humrat and Feinan units (Figure not shown), however, the range of $^{147}Sm/^{144}Nd$ ratios varies from 0.085 to 0.153, reflecting small differences in the LREE enrichment of these rocks. Regardless of these variations, the calculated epsilon neodymium values are all positive, and range from Nd = + 2.9 to + 5.4, where the averages of all units fall between 4 and 5, which implies that these rocks are enriched in the radiogenic ^{143}Nd relative to CHUR, i.e. derived from a magma depleted source in the mantle. The separation time of the Neoproterozoic samples of the crust from the magma reservoir in the mantle was determined by the model dates. They vary from 0.72 to 1.06 Ga with an average of 0.80 Ga for all units, indicating a recycled crust (McCulloch and Wasserburg, 1978; and Faure and Mensing, 2005).

Table 4. Rb-Sr and Sm-Nd data.

Sample [a]		$(^{87}Sr/^{86}Sr)^{b}$	Error	$(^{87}Sr/^{86}Sr)_{(T)}{}^{c}$	$(^{143}Nd/^{144}Nd)^{b}$	Error	$\varepsilon Nd_{(T)}{}^{c}$
Humrat alkali granite	NF1	0.783924	5	*0.71508*	0.512491	5	3.3
	NF7	0.731589	6	*0.70560*	0.512492	12	4.5
	NF11	0.808411	5	0.71909	0.512560	5	5.0
	NF12	0.751945	5	*0.70689*	0.512560	5	4.5
	NF45	0.800944	9	0.71734	0.512568	5	4.9
	NF54	0.902443	6	0.74084	0.512666	5	3.9
	NF59	0.762831	7	*0.70735*	0.512615	4	2.9
Mubarak alkali granite	NF10	1.011152	12	0.76418	0.512551	4	4.9
	NF14				0.512508	5	4.6
	NF39	0.769070	8	*0.70767*	0.512506	5	3.6
	NF40	0.785619	4	*0.71127*	0.512522	5	4.9
	NF41	1.270335	7	0.71058	0.512626	5	5.4
Feinan alkali granite	NF16				0.512543	5	3.8
	NF21	0.716882	9	*0.70373*	0.512427	5	4.4
	NF23	0.741231	6	*0.70894*	0.512480	5	4.2
	NF26	0.715448	9	*0.70146*	0.512483	5	4.0
	NF28	0.707734	6	*0.70411*	0.512481	5	4.1
	NF31	0.751308	7	*0.70789*	0.512426	4	4.5
	NF35	0.799512	8	*0.71264*	0.512484	3	3.3
Sabil granodiorite	NF8	0.707482	5	*0.70392*	0.512458	5	3.7
	NF47	0.704731	6	*0.70364*	0.512558	5	4.6
	NF48	0.709092	7	*0.70424*	0.512500	4	4.0
	NF52	0.706791	6	*0.70316*	0.512471	5	3.8

Article in Press: JJEES 16(2), June 2025.
This article has been accepted for publication and will appear in the upcoming issue. The final published version will be available through the journal website after copyediting, typesetting and proofreading. ©2025 JJEES.

	NF53	0.711007	5	*0.70376*	0.512449	5	3.7

a. Samples were dissolved with concentrated HF for four days at 160 °C on the hot plate. Digested samples were dried and taken up in 6N HCl. Sr and Nd were separated and purified using ion-exchange chromatography as described in Romer et al. (2005).
b. $^{87}Sr/^{86}Sr$ and $^{143}Nd/^{144}Nd$, normalized to $^{86}Sr/^{88}Sr = 0.1194$ and $^{146}Nd/^{144}Nd = 0.7219$, respectively, Sr was analyzed on a VG54Sector, a Finnigan MAT262 or a Triton multi-collector mass-spectrometer commonly using dynamic multicollection. Nd isotope data were obtained on a Finnigan MAT262 multi-collector mass-spectrometer using dynamic multicollection. Analytical uncertainties are given at $2\sigma_m$ level.
c. $^{87}Sr/^{86}Sr$ (T) and εNd (T) were calculated for the stratigraphic age using $\lambda(^{87}Rb) = 1.42 \times 10^{-11}\ y^{-1}$ and $\lambda\ (^{147}Sm) = 6.54 \times 10^{-12}\ y^{-1}$, $(^{147}Sm/^{144}Nd)_0$ CHUR = 0.1967, and $(^{143}Nd/^{144}Nd)_0$ CHUR = 0.512638, respectively, and the concentration data given in tables 4-1, 2 and 3. The italic values are calculated for $^{87}Rb/^{86}Sr$ ratios less than 4(Stoeser and Frost, 2006)

8. Discussion

8.1. age constraints

The U–Pb age spectra obtained for the investigated granitiods are restricted to three periods: 615, 603-601, and 586 Ma, for Sabil, Feinan-Mubarak, and Humrat, respectively (Table 1 and Figure. 14). The Sabil granodiorite belongs to the post-collisional calc-alkaline magmatic stage and is clearly intruded by the Abu-Jadda granite (596 Ma, Jarrar et al. 2017), Mubarak and Humrat granites of this study. On the other hand, the ages of Feinan and Mubarak granites coincide within analytical errors with the ages of the composite, andesite, and rhyolitic dikes dated by Ghanem et al. (2020) at 607, 594, and 600 Ma, respectively. The ages of these granitoids and the dikes postdate the Araba Unconformity placed at ca. 605 Ma (Powell et al. 2015) and falls within the extension-related felsic plutonic magmatic activity of the Araba Complex (Jarrar et al. 2003). The Humrat granite dated 586 ± 16 Ma truncates all of the above mentioned granitoids and dikes and is itself cross-cut mainly by dolerites dated at 579 Ma (Ghanem et al. 2020) and rarely by andesite dikes not dated yet. There is no field evidence for plutonic unit younger than the Humrat granite (Jarrar, et al., 2003).

Generally, the zircon ages of the dated rocks in southwestern Jordan, in this study, are well correlated with their equivalent plutonic U-Pb range ages from the northern part of the Eastern Desert of Egypt, northern and southern part of Sinai. Possible equivalents of the Jordanian granites of the Araba Complex have been dated at 580 to 608 Ma in the Eastern Desert and on Sinai and elsewhere in the northern ANS using conventional and SHRIMP zircon methods (e.g., Be'eri-Shlevin, et al., 2009 b; Wilde and Youssef, 2000; Mousa, et al., 2008; Breitkreuz, et al., 2010 and Be'eri-Shlevin, et al., 2010; Eyal et al., 2019).

The previously reported Rb-Sr ages for the investigated rocks in Lenz, et al. (1972); Jarrar et al. (1983); Jarrar et al. (2008); Brook et al. (1990) and elsewhere in the ANS (e.g., Wilde and Youssef, 2000; and Be'eri-Shlevin, et al., 2009), are younger than the U-Pb ages by 20 to 30 Ma. This result could be

attributed to many factors among which are the closure temperature of the Rb-Sr system and the sensitivity of the Rb-Sr system to weathering processes. Nevertheless, the reported age, e.g., 610 Ma of the Sabil granodiorite after Brook, et al. (1990), are younger than the uranium-lead age of the same rocks by 5 Ma.

8.2. Origin of intermediate and silicic magmas (Petrogenesis)

8.2.1. Evidence from Sr and Nd isotope ratios

The overlap in the $\varepsilon Nd_{(586-603\ Ma)}$ values for alkaline granites (+ 2.9 to + 5.4) and Sabil granodiorite $\varepsilon Nd_{(615\ Ma)}$ (+ 3.7 to + 4.6) (Table 4), suggest a genetic relation between the two magmas. It goes along with the low initial $^{87}Sr/^{86}Sr$ (~0.70374), as well as the high Nd content (~28ppm) of the post-collisional granitoids that could have been generated by small degree of partial melting of older island arc juvenile crust or by protracted fractional crystallization of mantle-derived parental mafic magma at about > 615 Ma (Smith, et al., 1999; and Jarrar, et al., 2003). The latter possibility should be abandoned due to the age difference of 15 to 30 Ma between the two suites.

The Nd model ages of the post-collisional and the extension-related Neoproterozoic rocks from south Jordan are similar, from 720 to 1060 Ma with an average of 800 Ma for all units (Table 4), suggesting little or no Archean or early to middle Proterozoic rocks contribution to the lower to middle crust of the northern ANS as has been documented by many investigators (Be'eri-Shlevin et al., 2009a; Liégeois and Stern, 2009; and Eyal, et al., 2010).

8.2.2. Geochemical evidence

8.2.2.1. Calc-alkaline suite

The calc-alkaline Sabil granodiorite is characterized by moderate to strong LREE enrichment but remain roughly parallel ((La/Lu)n = 8 - 26) and smooth without significant cross overs relative to the alkali granitoids among the three multi-elements patterns. The changes in the trace elements concentrations ratios are very small. The enrichments are obvious in Sr, Ba, P, Zr, Ti, Cr, Co, and Ni and show well-developed depletion in K, Rb, Th, Ta, Nb and Y. Furthermore, the Sabil granodiorites lack prominent Eu anomaly (Eu/Eu* = 0.7 - 1.0) that's typically observed in the alkali feldspar granites. Furthermore, these granodiorites are of Magnesian character in the sense of Frost et al. (2001) and display the strongest Ta-Nb anomaly.

These features are typical of subduction zone tectonic environment (Pearce, et al., 1984) and suggest a depleted lithospheric mantle source with some subducted crustal component (Whalen, et al., 1987; Eby, 1990; Smith, et al., 1999; and Auwera, et al., 2003). Nevertheless, the steep REE patterns of the granodiorite call for involvement of a garnet-bearing magma source like garnet-bearing mafic granulite of the lower crust. These garnet-granulites are documented as lower crustal xenoliths in Harrat Ash Sham Cenozoic basalts (Al-Zubi, 2015, unpubl. MSc Thesis).

8.2.2.2. Alkaline suite

The felsic end members in the Araba Complex, e.g. the Feinan-Mubarak and Humrat alkali feldspar granites suite rocks, share common features that hint to their origin. They are distinguished by high SiO_2 (~ 66 – 78 %), Na_2O +K_2O, Fe/Mg, and ΣREE (~ 86 – 472 ppm), enrichment in Zr, Nb, Y, Rb, Ta, and K, and low CaO, Ba, Sr, Ti, and P (Table 1), along with much lower Eu/Eu* values (0.06–0.85). Furthermore, they follow a gently sloping LREE ((La/Sm)n = ~ 2 - 8) and almost flat HREE ((Gd/Lu)n = ~ 0.3 – 1.7) chondrite-normalized patterns except the Mubarak which have a concave upwards HREE pattern. These geochemical features are very distinctive signature of the A-type granites (Whalen, et al., 1996; Landenberger and Collins, 1996).

On the other hand, the juxtaposition of both calc-alkaline and alkali granitoids in several locations in the Jordanian basement, e.g. Wadi ES-Sabil, overlap in their REE patterns and multi-elements plots (Figures. 9 and 11), and their relatively close U–Pb ages obtained from this study could be similar to the Sabil calc-alkaline granodiorite could fractionate to produce the alkaline granitoids. The REE pattern (Figure. 9 C) of the Mubarak granite and the The Dy/Dy* vs. Dy/Yb plot (Figure. 10) demonstrate that the evolution of the magmas of rocks could have resulted from the fractionation of amphiboles and pyroxenes.

Experiments of Sisson, et al. (2005) demonstrated the possible formation of A-type granite magma by a partial melting of K-rich basalt rocks in the middle and lower crust. Eyal et al. 2010 advocated this for the formation of A-type granites in Sinai Peninsula.

All investigated granitoids fall mostly in the field of slab-failure (Whalen and Hildebrad, 2019) on the tectonic discrimination diagrams of granites of Pearce et al. (1984, 1995). Slab failure at the end of the East African Orogeny and a consequent asthenospheric upwelling could have triggered decompresion melting of the subcontinental lithosphere and the lower over-thickened continental crust. Fractionation of these magmas with possible minor assimilation of crustal material resulted in the formation of the different granitoidal units. Possible fractionated material of similar age, within analytical error, to the alkaline units (Feinan, Mubarak and Humrat) can be found in the gabbro-diorite intrusions in Wadi Qunaia (Ghanem and Jarrar, 2013) and the quartz diorite of Wadi Mureihil, Central Wadi Araba (Jarrar and Ghanem, 2021).

9. Summary and conclusions

The following conclusions, arranged in order of importance, can be drawn from this study:

1. The obtained conventional U-Pb zircon ages are ~ 616, ~ 603, ~601, and ~ 586 Ma for the Sabil granodiorite Feinan, Mubarak, and Humrat units, respectively.
2. The investigated rocks are divided into two groups: the alkaline group, which includes the Humrat, Mubarak and Feinan alkali granite units of the Araba Complex; and the high-K calc-alkaline Sabil granodiorite unit from the Aqaba Complex.
3. The calc-alkaline Sabil granodiorite unit is of Magnesian character and mostly metaluminous; while the alkaline group is mostly of ferroan affinity, A-type, and mostly slightly peraluminous.
4. The alkaline suite is characterized of high SiO_2, Na_2O +K_2O, Fe/Mg, enrichment in Zr, Nb, Y, Rb, Ta, K and REE contents, and low CaO, Ba, Sr, Ti and P along with prominent negative Europium anomaly. Furthermore, they follow a gently sloping LREE and almost flat HREE chondrites patterns, except for the concave pattern of the Mubarak unit. They bear a close resemblance to within plate A-type granites.
5. The calc-alkaline Sabil unit and to a lesser degree the Feinan units show a Nb-Ta anomaly that's characteristic for volcanic arc granites (VAG) while the Mubarak and Humrat are more within plate granites. However, all of the units fall in the field of slab-failure in the sense of Whalen and Hildebrand (2019).

6. The εNd values of the alkali units ranged (+ 2.9 to + 5.4) and overlap with the εNd values of the Sabil granodiorite (+ 3.7 to + 4.6) with low initial $^{87}Sr/^{86}Sr$ (~0.70374).
7. The Zr geothermometer constrains the temperatures of crystallization between 800 to 950◦C. This roughly close to temperatures obtained by modeled crystallization sequence of the investigated units. The modeled mineralogy is shown only for the Sabil granodiorite unit.
8. The investigated suite could have been produced through decompressional partial melting of the subcontinental lithosphere and lower continental with fractional crystallization and minor crustal assimilation.
9. The Sabil granodiorite belongs to the calc-alkaline phase of the Aqaba Complex; the Feinan and Mubarak units represent the transition to the alkaline within-plate magmatism, while the Humrat is a truly A-type within plate alkali-feldspar granite.
10. The transitional magmatism coincides or slightly post-dates with the Araba Unconformity and the extensive dike swarms.

Acknowledgements

This paper is a part of the PhD thesis of the senior author. The logistic and financial support provided to the lead author by the Deanship of the Scientific Research and the Department of Geology at The University of Jordan, is highly appreciated. The lab work including microprobe analysis, isotopic analysis and age determination, and bulk chemistry has been conducted at the Helmholtz Center Potsdam-German Research Center for Geosciences (**G**eo**F**orschungs**Z**entrum (**GFZ**) during a six-month research stay of the senior author that has been financially supported by the Deutscher Akademisher Austausch Dienst (DAAD). The support of both institutions is gratefully acknowledged. Dr. Hind Ghanem kindly carried out microprobe analyses for selected samples at the Institute for Mineralogy and Crystallography, University of Stuttgart, Germany.

References

Abu El-Enen, M.M., Whitehouse, M.J., 2013. The Feiran–Solaf metamorphic complex, Sinai, Egypt: Geochronological and geochemical constraints on its evolution. Precambrian Research 239, 106-125.

Al-Zubi, R. 2015. A suite of upper mantle and lower crustal xenoliths form Harrat Ash Shaam, NE Jordan: mineralogy, geochemistry, and petrogenesis. Unpubl. MSc Thesis, The University of Jordan. 178 pp.

Beyth M, Stern RJ, Altherr R, Kröner A (1994) The late Precambrian Timna igneous complex, Southern Israel: Evidence for comagmatic-type sanukitoid monzodiorite and alkali granite magma. Lithos, **31**, 103 - 124.

Boyd, R., Nordgulen, Ø., Thomas, R.J., Bingen, B., Bjerkgard, T., Grenne, T., Henderson, I., Melezhik, V.A., Often, M., Sandstad, J.S., Solli, A., Tveten, E., Viola, G., Key, R.M., Smith, R.A., Gonzalez, E., Hollick, L.J., Jacobs, J., Jamal, D., Motuza, G., Bauer, W., Daudi, E., Feitio, P., Manhica, V., Moniz, A. and Rosse, D. (2010), The geology and geochemistry of the East African Orogen in the Northeastern Mozambique. South African Journal of Geology, 113 (1), 87-129.

Brook M, Ibrahim K, McCourt W (1990) New geochronological data from the Arabian Shield area of southwest Jordan. In: Proceedings of the 3rd Jordanian Geological. Conference, Amman, Jordan. pp 361-394

Davidson, J., Turner, S., and Plank, T. 2013. Dy/Dy*: variations arising from mantle sources and petrogenetic processes. Journal of Petrology 54, 525-537.

Dulski, P. (2001), Reference Materials for Geochemical studies: New Analytical Data by ICP-MS and critical discussion of reference values. Geostandard Newsletters25, 97-125.

Eby, GN. (1990) The A-type granitoids: A review of their occurrence and chemical characteristics and speculations on their petrogenesis. Lithos, 26, 115-134.

El-Bialy MZ , Hassen I (2012) The late Ediacaran (580-590 Ma) onset of anorogenic alkaline magmatism in the Arabian-Nubian Shield: Katherina A-type rhyolites of Gabal Ma'ain, Sinai, Egypt. Precambrian Research 2012-2016, 1-22.

Elisha B, Katzir, Y, Kylander-Clark, A (2017) Ediacaran (~620 Ma) high-grade regional metamorphism in the northern Arabian Nubian Shield: U-Th-Pb monazite ages of the Elat schist. Precambrian Research 295, 172-186.

Elisha B, Katzir Y, Kylander-Clark ARC, Golan T (2019) The timing of migmatization in the northern Arabian-Nubian Shield: Evidence for a juvenile sedimentary component in collision-related batholiths. Journal of Metamorphic Geology 37, 591-610.

Eyal, M., Litvinovsky, B., Jahn, B.M., Zanvilevich, A., Katzir, Y., 2010. Origin and evolution of post-collisional magmatism: Coeval Neoproterozoic calc-alkaline and alkaline suites of the Sinai Peninsula. Chemical Geology 269, 153-179.

Eyal Y, Eyal M, Litvinovsky B, Jahn Bm, Calvo R, Golan T (2019) The evolution of the Neoproterozoic Elat Metamorphic Complex, northernmost Arabian-Nubian Shield: Island arc to syncollisional stage and post-collisional magmatism. Precambrian Research 320:137-170

Faure, G. and Mensing, T. M. (2005), Isotopes: Principles and Applications. John Wiley & Sons.

Frost, B. R., Arculus, R. J., Barnes, C. G., Collins,W. J., Ellis, D. J. & Frost, C. D. (2001). A geochemical classification of granitic rocks. Journal of Petrology 42, 2033-2048

Frost, BR and Frost CD. (2008) A Geochemical Classification for Feldspathic Igneous Rocks. Journal of Petrology, 49, Issue 11, 1955–1969, https://doi.org/10.1093/petrology/egn054

Garfunkel Z (1999) History and paleogeography during the Pan-African orogen to stable platform transition: reappraisal of the evidence from the Elat area and the northern Arabian-Nubian Shield. Isr. J. Earth Sci. 48:135-157

Ghanem, H. & Jarrar., G. 2013. Geochemistry and Petrogenesis of the 595 Ma Qunai Monzogabbro, Jordan. Journal of African Earth Sciences 88, 1-14.

Ghanem H, McAleer RJ, Jarrar GH, Al Hseinat Ma, Whitehouse M (2020) $^{40}Ar/^{39}Ar$ and U-Pb SIMS zircon ages of Ediacaran dikes from the Arabian-Nubian Shield of south Jordan. Precambrian Res. 343:105714

Ghanem H, Jarrar GH, McAleer, RJ Passchier CW, Thomas , Whitehouse MJ, Wintsch, RP(2022): Drowned in granite - retrieving the tectono-metamorphic history of the Janub metamorphic complex, the northernmost part of the Arabian-Nubian Shield. Precambrian Research 106903, vol 383. https://doi.org/10.1016/j.precamres.2022

Ghiorso, M. S. and Gualda, G.A. R. (2015) An H2O-CO2 mixed fluid saturation model compatible with rhyolite-MELTS. Contributions to Mineralogy and Petrology, 169:53. DOI 10.1007/s00410-015-1141-8.

Habboush, M. A. and Jarrar, G. (2009). Petrology and geochemistry of the metasediments of the Janub metamorphic suite, southern Jordan: Implications for geothermobarometry and economic potential. Jordan Journal of Earth and Environmental Sciences. Vol 2, No.1, 7-17.

Harris, NBW, Pearce, JA, Tendle AG (1986). Geochemical characteristics of collision-zone magmatism. In: Coward MP, Ries AC, (eds) Collision tectonics, vol 19,Special publication of the Geological Society of London., pp 67-81. http://doi.org/10.1144.GSI. SP 1986 019.01.04.

Ibrahim KM and McCourt WJ (1995) Neoproterozoic granitic magmatism and tectonic evolution of the northern Arabian Shield: Evidence from Southwest Jordan. J Afr Earth Sci, **20**, 103-118

Jarrar, GH., Baumann, A. and Wachendorf, H. (1983), Age determinations in the Precambrian basement of the Wadi Araba area southwest Jordan. Earth and planetary Science letters, 63: 292-304.

Jarrar GH (1995) Pan-African Amphibolites from SW-Jordan. Chemie Der Erde-Geochemistry 55(1):31-45

Jarrar GH (1998) Mineral chemistry in dioritic hornblendites from Wadi Araba, southwest Jordan. J. Afr. Earth Sci. 26(2):285-295

Jarrar, GH, Stern, R. J., Saffarini, G. and Al-Zubi, H. (2003), Late- and post-orogenic Neoproterozoic intrusions of Jordan: implications for crustal growth in the northmost segment of the East African Orogen. Precambrian Research, 123: 295-319.

Jarrar GH, Saffarini G, Baumann A, Wachendorf H (2004) Origin, age and petrogenesis of Neoproterozoic composite dikes from the Arabian-Nubian Shield, SW Jordan. Geol. J. 39(2):157-178

Jarrar, GH., Manton, W., Stern, R. and Zachmann, D. (2008), Late Neoproterozoic A-type granites in the Northernmost Arabian-Nubian Shield formed by fractionation of basaltic melts. Chemie der Erde-Geochemistry, 68: 295-312.

Jarrar, GH., Theye, T., Yaseen, N., Whitehouse, M., Pease, V., Passchier, C., 2013a. Geochemistry and P–T–t evolution of the Abu-Barqa Metamorphic Suite, SW Jordan, and implications for the tectonics of the northern Arabian–Nubian Shield. Precambrian Research 239, 56-78.

Jarrar GH, Yaseen N, Theye T (2013b) A hybrid composite dike suite from the northern Arabian Nubian Shield, southwest Jordan: Implications for magma mixing and partial melting of granite by mafic magma. J. Volcanol. Geotherm. Res. 254:80-93

Jarrar G.H., Stern R.J., Theye T., Yaseen N., Pease V., Miller N., Ibrahim K.M., Passchier C.W., Whitehouse M. 2017. Neoproterozoic Rosetta Gabbro from northernmost Arabian–Nubian Shield, south Jordan: Geochemistry and petrogenesis. Lithos. 284-285:545-559.

Jarrar, GH. and Ghanem, (2021) Neoproterozoic Crustal Evolution of the Northernmost Arabian-Nubian Shield, South Jordan. Chapter five in a book The Geology of the Arabian-Nubian Shield, Regional geology reviews, Springer Verlag. 109-137;https://doi.org/10.1007/978-3-03

Johannes W and Holtz 1996. Petrogenesis and experimental petrology of granitic rocks. Springer Verlag.

Johnson PR, Halverson GP, Kusky TM, Stern RJ, Pease V (2013) Volcanosedimentary Basins in the Arabian-Nubian Shield: Markers of Repeated Exhumation and Denudation in a Neoproterozoic Accretionary Orogen. Geosciences 3(3):389-445

Kröner A, Stern R (2004) Pan-African orogeny. In: Selley RC, Cocks LRM, Plimer IR (eds) Encyclopedia of Geology. Elsevier, Amsterdam., pp 1-12

Lenz, H., Bender, F., Besang, C., Harre, W., Kreuzer, H., Mueller, P. and Wendt, I. (1972), The age of early tectonic events in the zone of the Jordan Geosuture based on radiometric data. 24th International Geological Congress, 3: 371-379.

McCourt, W.J. and Ibrahim, K. (1990), The Geology, Geochemistry and Tectonic setting of the Granitic and Associated Rocks in the Aqaba and Araba Complexes of Southwest Jordan. Natural Resources Authority, Geological Directorate, Geological Mapping Division, Bulletin 10, Amman.

Mousa, E. M. M., Stern, R. J., Manton, W. I. and Kamal, A. (2008), SHRIMP zircon dating and Sm-Nd isotopic investigations of Neoproterozoic granitoids, Eastern Desert, Egypt. Precambrian Research, 160: 341-356.

Moyen, J.-F., Laurent O, Chelle-Michou, C., Couzini, S., Vanderhaege, O., Zeh, A., Villaros, Gardien, V. (2017) Collision vs. subduction-related magmatism: Two contrasting ways of granite formation and implications for crustal growth. Lihos, 277, 154-177.

Pallister, J.S. Stacey, J.S. , Fisher L.B. , PREMO, W. R. (1988). Precambrian ophiolites of Arabia: Geologic settings, U-Pb geochronology, Pb-isotope characteristics, and implications for continental accretion. Precambrian Research, 38, 1-54.

Pearce, J.A., Harris N.B.W., Tendle, A.G. (1984) Trace elements discrimination diagrams for the tectonic interpretation of granitic rocks. Journal of Petrology 25: 956-983.

Powell JH, Abed AM, Le Nindre Y-M (2014) Cambrian stratigraphy of Jordan. Geoarabia 19(3):81-134

Powell JH, Abed A, Jarrar GH (2015) Ediacaran Araba Complex of Jordan. Geoarabia 20(1):99-156

Romer, R. L., Schärer, U. and Steck, A. (1996), Alpine and pre-Alpine magmatism in the root-zone of the western central Alps.Contributions to Mineralogy and Petrology, 123, 138–158.

Romer, R. L., Heinrich, W., Schröder-Smeibidl, B., Meixner, A., Fischer, C. O. and Schulz, C. (2005), Elemental dispersion and stable isotope fractionation during reactive fluid-flow and fluid immiscibility in the Bufa del Diente aureole, NE-Mexico: Evidence from radiographies and Li, B, Sr, Nd, and Pb isotope systematics. Contributions to Mineralogy and Petrology, 149 (4), 400-429.

Romer, R. L. and Hahne, K. (2010), Life of the Rheic Ocean: scrolling through the shale record, Gondwana Research, 17 (2-3), 236-253.

Schmid, R., Romer, R. L., Franz, L., Oberhänsli, R. and Martinotti, G. (2003), Basement-Cover Sequences within the UHP unit of the Dabie Shan. Journal of Metamorphic Geology, 21 (6), 531-538.

Schmidt, C., Bruhn, D. and Wirth, R. (2003), Experimental evidence of transformation plasticity in silicates: minimum of creep strength in quartz. Earth and Planetary Science letters, 205, 273–280.

Steiger RH and Jager E (1977) Subcommission on geochronology: convention on the use of decay constants in geo- and cosmo-chronology. Earth Planet Sci Letters 36:359-362

Stern, R.J., 1994. Arc assembly and continental collision in the Neoproterozoic East African Orogen: implications for the consolidation of Gondwanaland. Annual Review of Earth and Planetary Sciences 22, 319-351.

Tang, Y-W, Chen, L, Zhao, Z-F, Zheng, Y-F. (2020) Geochemical evidence for the production of granitoids through reworking of the juvenile mafic crust in the Gangdese Orogen, southern Tibet. Geological Society of America Bulletin, 132, 1374-1364.

Wachendorf H, Zachmann D, Jarrar G (1985) The role of pressure in control of potassium, sodium, and copper concentration in hypabyssal intrusives as demonstrated in late Precambrian dikes in southwest Jordan. Precambrian Res. 30(3):221-248

Whalen, JB, Currie KL, Chappell, BW. (1987). A-type granites: geochemical characteristics, discrimination and petrogenesis. Contributions to Mineralogy and Petrology. 95: 407-419.

Whalen, JB, Jenner, GA, Longstaffe, FJ., Robert, F., Cartiepy, C. 1996. Geochemical and isotopic (O, Nd, Pb and Sr) constraints on A-type granite petrogenesis based on the Topsails igneous suite, Newfoundland Appalations. Journal of Petrology, 37, 1463-1489

Whalen JB, Hildebrand RS (2019) Trace elements discrimination of arc, slab failure, and A-type granitic rocks. Lithos, 348-349, 105 105179. https://doi.org/10.1016/j.lithos.2019.105179